Stem Cell Reports
Article

OPEN ACCESS

Lineage Tracing Reveals the Bipotency of SOX9$^+$ Hepatocytes during Liver Regeneration

Ximeng Han,[1,2,3,10] Yue Wang,[1,2,10] Wenjuan Pu,[1,2] Xiuzhen Huang,[1,2] Lin Qiu,[2] Yan Li,[1,2] Wei Yu,[1,2] Huan Zhao,[1,2] Xiuxiu Liu,[1] Lingjuan He,[1,2] Libo Zhang,[1,2] Yong Ji,[4,5] Jie Lu,[6,*] Kathy O. Lui,[7] and Bin Zhou[1,2,3,4,8,9,*]

[1]The State Key Laboratory of Cell Biology, CAS Center for Excellence in Molecular Cell Science, Shanghai Institute of Biochemistry and Cell Biology, Chinese Academy of Sciences, University of Chinese Academy of Sciences, Shanghai 200031, China
[2]Key Laboratory of Nutrition and Metabolism, Institute of Nutrition and Health, Shanghai Institutes for Biological Sciences, Chinese Academy of Sciences, University of Chinese Academy of Sciences, Shanghai 200031, China
[3]School of Life Science and Technology, ShanghaiTech University, Shanghai 201210, China
[4]The Collaborative Innovation Center for Cardiovascular Disease Translational Medicine, Nanjing Medical University, Nanjing 211100, China
[5]Key Laboratory of Cardiovascular and Cerebrovascular Medicine, Nanjing Medical University, Nanjing 211100, China
[6]Department of Gastroenterology, Shanghai 10th People's Hospital, Tongji University School of Medicine, Shanghai 200072, China
[7]Department of Chemical Pathology; Li Ka Shing Institute of Health Sciences, The Chinese University of Hong Kong, Prince of Wales Hospital, Shatin, Hong Kong SAR 999077, China
[8]Key Laboratory of Regenerative Medicine of Ministry of Education, Institute of Aging and Regenerative Medicine, Jinan University, Guangzhou 510632, China
[9]Institute for Stem Cell and Regeneration, Chinese Academy of Sciences, Beijing 100101, China
[10]Co-first author
*Correspondence: lujie791111@tongji.edu.cn (J.L.), zhoubin@sibs.ac.cn (B.Z.)
https://doi.org/10.1016/j.stemcr.2019.01.010

SUMMARY

Elucidation of the role of different cell lineages in the liver could offer avenues to drive liver regeneration. Previous studies showed that SOX9$^+$ hepatocytes can differentiate into ductal cells after liver injuries. It is unclear whether SOX9$^+$ hepatocytes are uni- or bipotent progenitors at a single-cell level during liver injury. Here, we developed a genetic tracing system to delineate the lineage potential of SOX9$^+$ hepatocytes during liver homeostasis and regeneration. Fate-mapping data showed that these SOX9$^+$ hepatocytes respond specifically to different liver injuries, with some contributing to a substantial number of ductal cells. Clonal analysis demonstrated that a single SOX9$^+$ hepatocyte gives rise to both hepatocytes and ductal cells after liver injury. This study provides direct evidence that SOX9$^+$ hepatocytes can serve as bipotent progenitors after liver injury, producing both hepatocytes and ductal cells for liver repair and regeneration.

INTRODUCTION

Under normal conditions the liver is an organ with slow parenchymal cell turnover, and the lifespan of hepatocytes can reach 200–300 days in a resting state. During homeostasis, it is generally believed that the liver lacks a multipotent stem cell population to maintain organ renewal, and thus ductal cells and hepatocytes are unipotent (Miyajima et al., 2014). Previous studies have indicated that facultative stem cells, also known as atypical ductal cells or oval cells, can differentiate into hepatocytes (Farber, 1956; Popper et al., 1957). Studies using Hnf1b or osteopontin (OPN) promoter-driven Cre fate mapping have suggested that liver progenitor cells or biliary epithelial cells could give rise to hepatocytes after liver injuries (Espanol-Suner et al., 2012; Rodrigo-Torres et al., 2014). However, recent lineage-tracing studies reported that virtually all hepatocytes are derived from pre-existing hepatocytes before injury rather than differentiating from stem cells (Grompe, 2014; Malato et al., 2011; Schaub et al., 2014; Wang et al., 2017; Yanger et al., 2014). Following severe chronic liver injury in which the proliferative potential of hepatocytes is significantly inhibited, a group of hepatic progenitor cells (HPCs) contribute significantly to the restoration of liver parenchyma, generating both hepatocytes and biliary epithelia (Lu et al., 2015). Indeed, following severe and chronic liver injuries that impair hepatocyte proliferation, committed ductal cells or cholangiocytes can act as facultative liver stem cells and generate hepatocytes for liver repair and regeneration (Deng et al., 2018; Raven et al., 2017). Conversely, hepatocytes can undergo hepatocyte-to-ductal cell transition after certain injuries (Yanger et al., 2013). In an animal model of human Alagille syndrome, hepatocytes could also convert into *de novo* mature biliary epithelial cells that form functional bile ducts (Schaub et al., 2018). Under chronic injury, mature hepatocytes could generate bipotential adult liver progenitors that give rise to both ductal cells and hepatocytes (Tarlow et al., 2014b). These studies indicated that mature hepatocytes or ductal cells could be reprogrammed into counterparts under certain conditions, as demonstrated in extremely severe liver injury models that promote cell-lineage conversion and cell plasticity. While these studies involved genetic lineage tracing at the population level, it remains unclear whether a single cell such as a hepatocyte is predetermined to give rise to hepatocytes, biliary epithelial cells, or both during

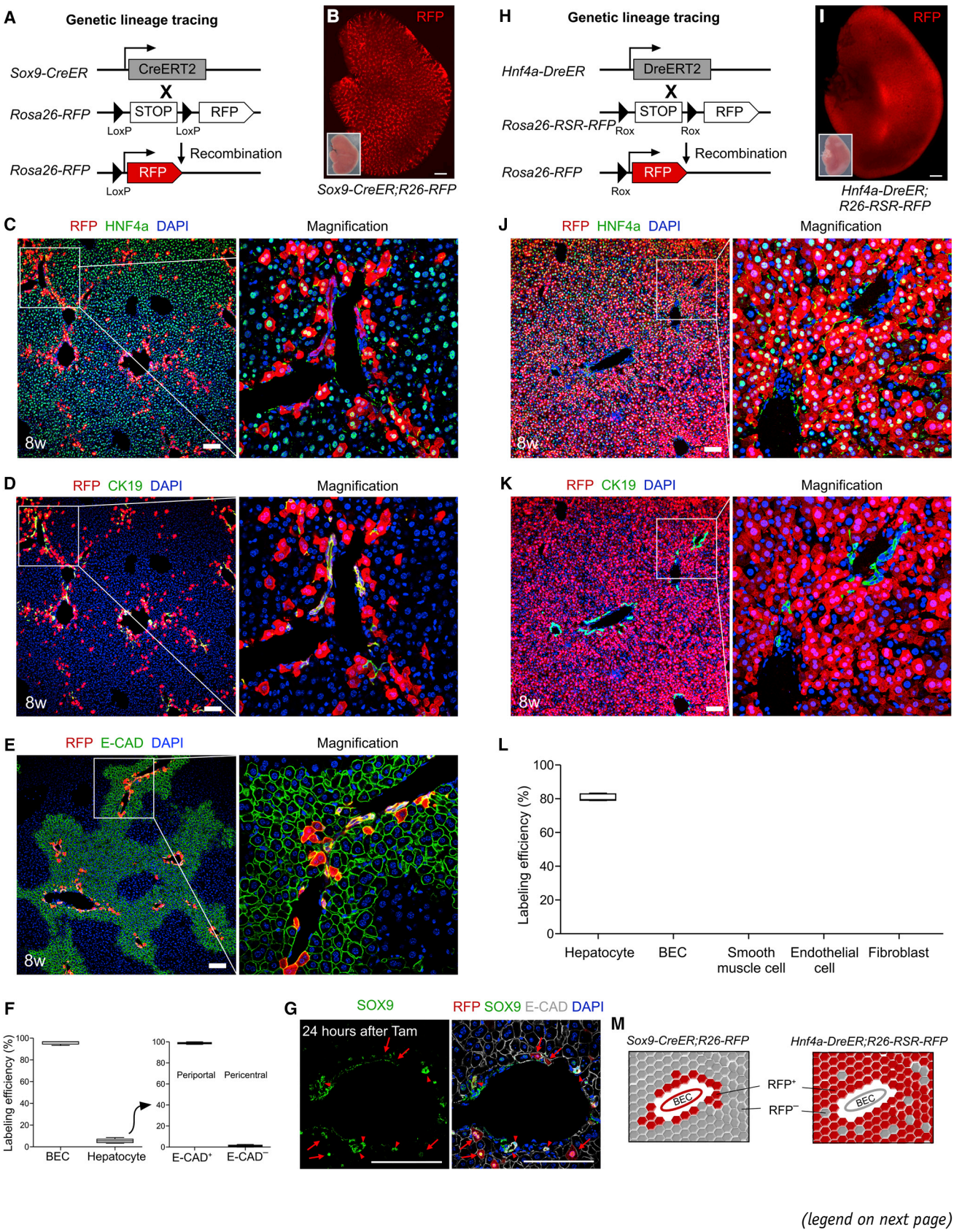

(legend on next page)

injury. Unraveling the potency and plasticity of committed hepatocytes may provide evidence to help elucidate the liver progenitor cell hierarchy and their roles in liver repair and regeneration.

Sox9 (sry-related high mobility group-box gene 9) is a family gene homolog located on the male Y chromosome (Suzuki et al., 2015). In the liver, SOX9 regulates the development of intrahepatic bile ducts through a mode of tubulogenesis (Antoniou et al., 2009). Furuyama et al. (2011) reported that SOX9$^+$ ductal epithelial cells are endogenous HPCs that contribute to hepatocytes during liver homeostasis and after injuries. Subsequent lineage-tracing studies using a multicolored fluorescent Confetti reporter showed that SOX9$^+$ cells contribute only minimally (<1%) to hepatocytes (Tarlow et al., 2014a). Because SOX9 is also expressed in a subset of hepatocytes, albeit at a lower level compared with that in ductal cells (Font-Burgada et al., 2015; Yanger et al., 2013), the rare contribution of SOX9$^+$ cells to hepatocytes could be due to prelabeled hepatocytes that express SOX9 (He et al., 2017). Indeed, these SOX9$^+$ hepatocytes undergo extensive proliferation and replenish liver mass after chronic liver injuries without giving rise to hepatocellular carcinoma (Font-Burgada et al., 2015), indicating that SOX9$^+$ hepatocytes could be an important source of hepatocytes with therapeutic potential. It remains unknown whether individual SOX9$^+$ hepatocytes are unipotent (ductal cell or hepatocyte lineage) or bipotent (both ductal cell and hepatocyte lineages) during liver injury and repair.

The genetic lineage-tracing technique is an effective method for unraveling cell fate in development, disease, and regeneration (Tian et al., 2015). The conventional genetic tracing method depends on a singular gene marker that may show low efficacy in defining one particular cell population. For example, *Sox9-CreER* targets both periportal hepatocytes and biliary epithelial cells. To achieve more precise labeling of cell lineages and trace their cell fate *in vivo*, we recently incorporated a recombination system, Dre-rox, to supplement Cre-loxP for enhancing the precision of genetic lineage tracing (He et al., 2017). In this study, we generated an intersectional genetic strategy showing that a subset of SOX9$^+$ hepatocytes, at the single-cell level, are bipotent progenitors that differentiate into both hepatocytes and biliary epithelial cells during liver injury and repair.

RESULTS

Characterization of *Sox9-CreER* and *Hnf4a-DreER* Mouse Lines

SOX9$^+$ hepatocytes express both SOX9 and hepatocyte markers, such as HNF4a, but do not express the biliary epithelial cell marker CK19 (He et al., 2017). For lineage tracing of SOX9$^+$HNF4a$^+$ hepatocytes, we generated two distinct mouse lines that utilize two orthogonal recombinases: *Sox9-CreER* and *Hnf4a-DreER*. The *Sox9-CreER* mouse was crossed with the *R26-RFP* reporter mouse to generate the *Sox9-CreER;R26-RFP* mouse. Tamoxifen induction led to Cre-loxP recombination, which resulted in permanent labeling of SOX9$^+$ cells and all their descendants (Figure 1A). Whole-mount fluorescence imaging of *Sox9-CreER;R26-RFP* livers showed that a substantial number of hepatic cells were labeled after tamoxifen induction (Figure 1B). Immunostaining for RFP, the hepatocyte marker HNF4a, or the ductal cell marker CK19 on *Sox9-CreER;R26-RFP* liver sections showed that RFP$^+$ cells were HNF4a$^+$ or CK19$^+$ (Figures 1C and 1D), indicating hepatocytes and ductal cells/biliary epithelial cells (BECs), respectively. Notably, most RFP$^+$ hepatocytes were close to the portal vein region where BECs were located, which is consistent with previous reports. Staining of the periportal hepatic zonation marker E-cadherin (E-CAD) verified that these SOX9$^+$ hepatocytes were periportal hepatocytes (Figure 1E). Quantification of hepatocyte labeling efficiency showed that 96.51% ± 0.38% of BECs were RFP$^+$ and 5.49% ± 1.93% of hepatocytes were RFP$^+$ (Figure 1F). Of these positive hepatocytes, almost all were positive for

Figure 1. Fate Mapping of Hepatic Cell Lineages by *Sox9-CreER* or *Hnf4a-DreER*

(A and H) Schematic figure showing lineage-tracing strategy by *Sox9-CreER;R26-RFP* (A) or *Hnf4a-DreER;R26-RSR-RFP* (H).

(B and I) Whole-mount fluorescence views of livers from 8-week-old adult mice. Tamoxifen was induced 4 days later. Insets indicate bright-field images.

(C and J) Immunostaining for RFP and HNF4a on liver sections.

(D and K) Immunostaining for RFP and CK19 on liver sections.

(E) Immunostaining for RFP and periportal hepatocyte marker E-CAD on liver sections.

(F) Quantification of the percentage of labeled CK19$^+$ biliary epithelial cells (BECs) or HNF4a$^+$ hepatocytes (left panel). The percentage of E-CAD$^+$ or E-CAD$^-$ cells in labeled hepatocytes is shown on the right panel. Data are mean ± SEM; n = 5.

(G) Immunostaining for SOX9, RFP, and periportal hepatocyte marker E-CAD on liver sections.

(L) Quantification of the percentage of labeled cells among different lineages. Data are mean ± SEM, n = 5.

(M) Cartoon image showing the fate mapping of hepatic cells by *Sox9-CreER* or *Hnf4a-DreER*. Scale bars, 1 mm (B and I) and 100 μm (C–E, G, J, and K).

E-CAD (>99%, Figure 1F), suggesting periportal hepatocytes. To confirm that SOX9 protein was indeed expressed in the hepatocytes in addition to BECs, we also collected the tissues 24 h after tamoxifen induction and stained them for RFP, SOX9, and E-CAD. We found that SOX9 was expressed in a subset of periportal hepatocytes (arrows) as well as BECs (arrowheads, Figure 1G).

We next generated an *Hnf4a-DreER* knockin mouse by placing the DreER cDNA in-frame with the initiating ATG of the *Hnf4a* gene (Figure S1A). The *Hnf4a-DreER* mouse was crossed with the *R26-rox-stop-rox-RFP* (*R26-RSR-RFP*) reporter to generate the *Hnf4a-DreER;R26-RSR-RFP* mouse. Tamoxifen treatment induced Dre-rox recombination, which removed the Stop cassette and led to RFP expression in HNF4a$^+$ hepatocytes (Figure 1H). Whole-mount fluorescence imaging of *Hnf4a-DreER;R26-RSR-RFP* mouse liver showed RFP$^+$ signals throughout the entire liver (Figure 1I). Immunostaining for RFP, HNF4a, CK19, or EpCAM on liver sections showed that HNF4a$^+$ hepatocytes were RFP$^+$, while CK19$^+$ or EpCAM$^+$ BECs were RFP$^-$ (Figures 1J, 1K, and S1B). We also stained other cell-lineage markers, such as desmin, α-smooth muscle actin (αSMA), VE-cadherin, platelet-derived growth factor receptor α (PDGFRα), and E-CAD, with RFP on liver sections and found that RFP$^+$ cells were parenchymal epithelial cells but not endothelial cells, smooth muscle cells, hepatic satellite cells, or fibroblasts (Figures S1C–S1G). Quantification of labeled cells showed that 80.25% ± 2.03% of hepatocytes were RFP$^+$ while other cell lineages did not express RFP in *Hnf4a-DreER;R26-RSR-RFP* (Figure 1L). Taken together, these data demonstrated that *Hnf4a-DreER* specifically and efficiently targeted hepatocytes in the liver. While *Sox9-CreER* labeled BECs and a subset of periportal hepatocytes, *Hnf4a-DreER* labeled only hepatocytes (Figure 1M); thus, SOX9$^+$HNF4a$^+$ hepatocytes could then be targeted by *Sox9-CreER* and *Hnf4a-DreER* dual recombinases.

Specific Labeling of SOX9$^+$ Hepatocytes by Dual Recombinases

To achieve specific labeling of SOX9$^+$ hepatocytes, we needed to target SOX9$^+$ HNF4a$^+$ cells in the liver by intersectional genetics (Figure 2A) so that the double-positive cell population could be distinguished from single positive cells. We crossed the characterized *Hnf4a-DreER* and *Sox9-CreER* mice with a dual recombinase-mediated RFP reporter (*R26-rox-Stop-rox-loxp-Stop-loxp-RFP*, as *R26-Ai66*) to generate the *Sox9-CreER;Hnf4a-DreER;R26-Ai66* triple-positive mouse line (Figure 2B). In this reporter line, activation of RFP required both Dre-rox and Cre-loxP recombination, which removed transcriptional Stop cassettes. Therefore, only SOX9$^+$HNF4a$^+$ hepatocytes that harbored both Cre and Dre recombinases could be genetically labeled (Figure 2B). With this genetic design, single positive cell populations, such as SOX9$^+$HNF4a$^-$ cells (BECs) or SOX9$^-$ HNF4a$^+$ hepatocytes, remained unlabeled (Figure 2B). One week after tamoxifen induction, livers were collected from *Sox9-CreER;Hnf4a-DreER;R26-Ai66* mice for analysis. Immunostaining of liver sections for CK19 and HNF4a showed labeling of hepatocytes in the periportal zone of the liver lobule, and BECs were RFP$^-$ (Figure 2C), demonstrating selective labeling of SOX9$^+$HNF4a$^+$ hepatocytes. We examined the littermate controls *Sox9-CreER;R26-Ai66* or *Hnf4a-DreER;R26-Ai66* and performed the same tamoxifen induction strategy and immunostaining for subsequent analysis. In both groups, no RFP$^+$ hepatocytes or BECs were detected (Figures 2D and 2E), demonstrating that RFP expression required both Cre-loxP and Dre-rox recombination. Taken together, these data demonstrated the successful generation of a mouse genetic tool for targeting SOX9$^+$ hepatocytes in the liver.

SOX9$^+$ Hepatocytes Expand Significantly after CCl_4-Induced Liver Injury

To examine the cell dynamics of SOX9$^+$ hepatocytes after liver injuries, we injected *Sox9-CreER;Hnf4a-DreER;R26-Ai66* mice with CCl_4 or performed a partial hepatectomy (PHx) to induce liver injuries. CCl_4 injury induces injury in the pericentral regions and stimulates the expansion of compensatory growth of periportal hepatocytes (Pu et al., 2016), while PHx induces more general hepatocyte growth throughout the liver, including hepatocyte hypertrophy and compensatory hepatocyte proliferation (Miyajima et al., 2014). Tamoxifen was induced at 8 weeks old, and after a 2-week washout period, mice were treated 10 times with CCl_4 and liver samples collected at 14 weeks (after injury) and 18 weeks (recovery group) for analysis (Figure 3A). Sirius red staining of liver sections showed strong fibrosis in the injured liver compared with that of the oil-treated control group, and tissue fibrosis was reduced in the recovery group 4 weeks after the last CCl_4 treatment (Figure 3B). Whole-mount fluorescent imaging of livers showed significant RFP signals in the injury and recovery group compared with the control group (Figure 3C). Immunostaining for CK19 and RFP showed that these RFP$^+$ cells did not contribute to CK19$^+$ BECs and remained as hepatocytes in the injured and recovered livers (Figure 3D). We also stained E-CAD in tissue sections of the control, CCl_4 injury, and recovery groups. We found that RFP$^+$ hepatocytes remained in zone 1 (E-CAD$^+$) before injury. During CCl_4 injury, the zone-1 marker E-CAD was expressed throughout the liver. After recovery the zonation was restored, with E-CAD expression restricted mainly to the periportal hepatocytes. Interestingly, a subset of the expanded RFP$^+$ hepatocytes extended to the pericentral regions and no longer maintained E-CAD expression, indicating reprogramming of SOX9-derived hepatocytes after

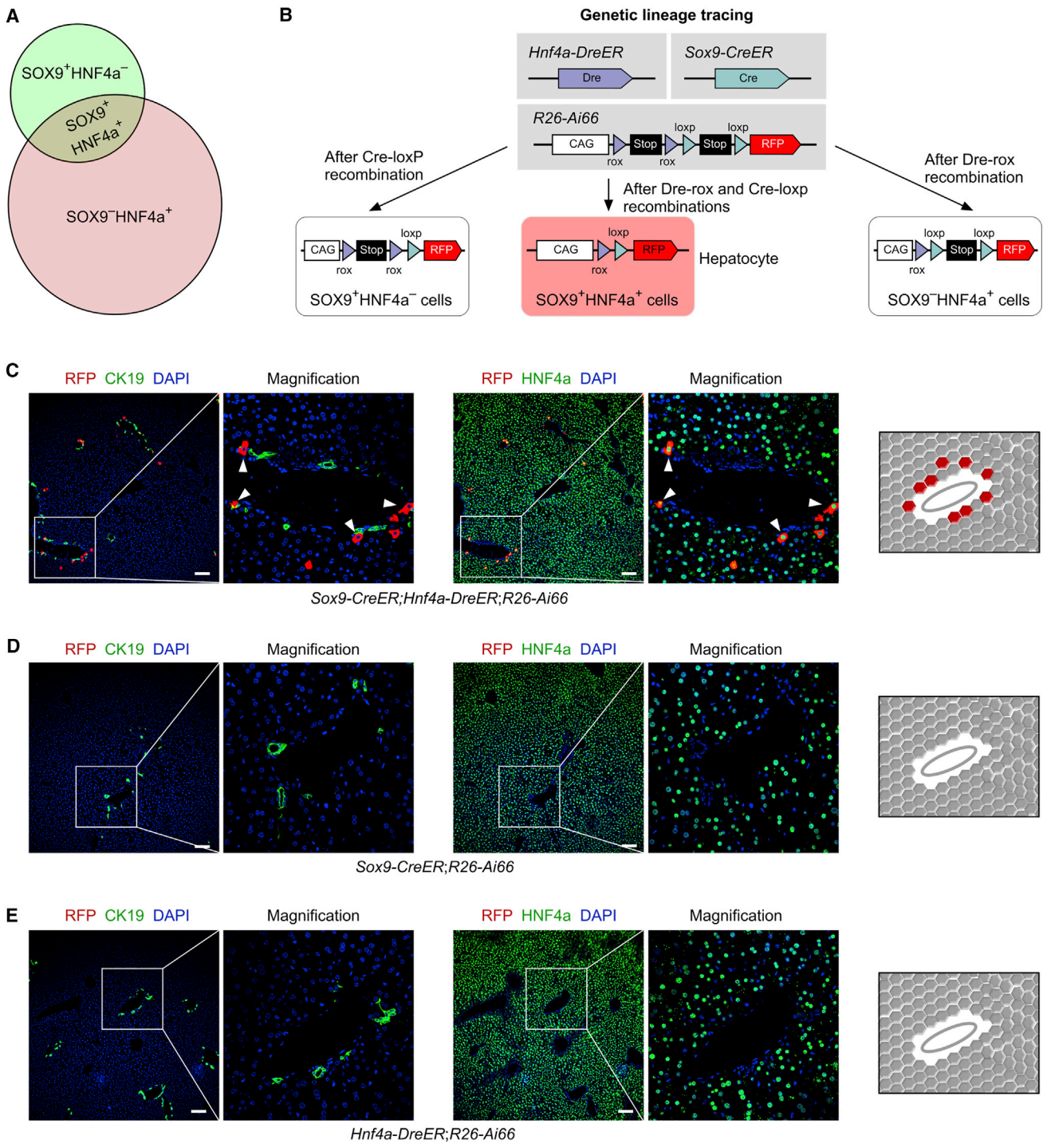

Figure 2. Lineage Tracing of SOX9$^+$ Hepatocytes by Dural Recombination

(A) Schematic showing intersectional genetics for labeling of double-positive cells (SOX9$^+$Hnf4a$^+$).

(B) Schematic showing lineage-tracing strategy by Dre-rox and Cre-loxP recombinations. Dural recombination, but not singular one, labels SOX9$^+$Hnf4a$^+$ hepatocytes.

(C–E) Immunostaining for RFP, CK19, and HNF4a on liver sections shows periportal RFP$^+$HNF4a$^+$ hepatocytes (arrowheads) in *Sox9-CreER;Hnf4a-DreER;R26-Ai66* (C) but not in *Sox9-CreER;R26-Ai66* (D) or *Hnf4a-DreER;R26-Ai66* (E) liver sections. Cartoon images on right panels show labeling result. Each figure is representative of five individual samples. Scale bars, 100 μm.

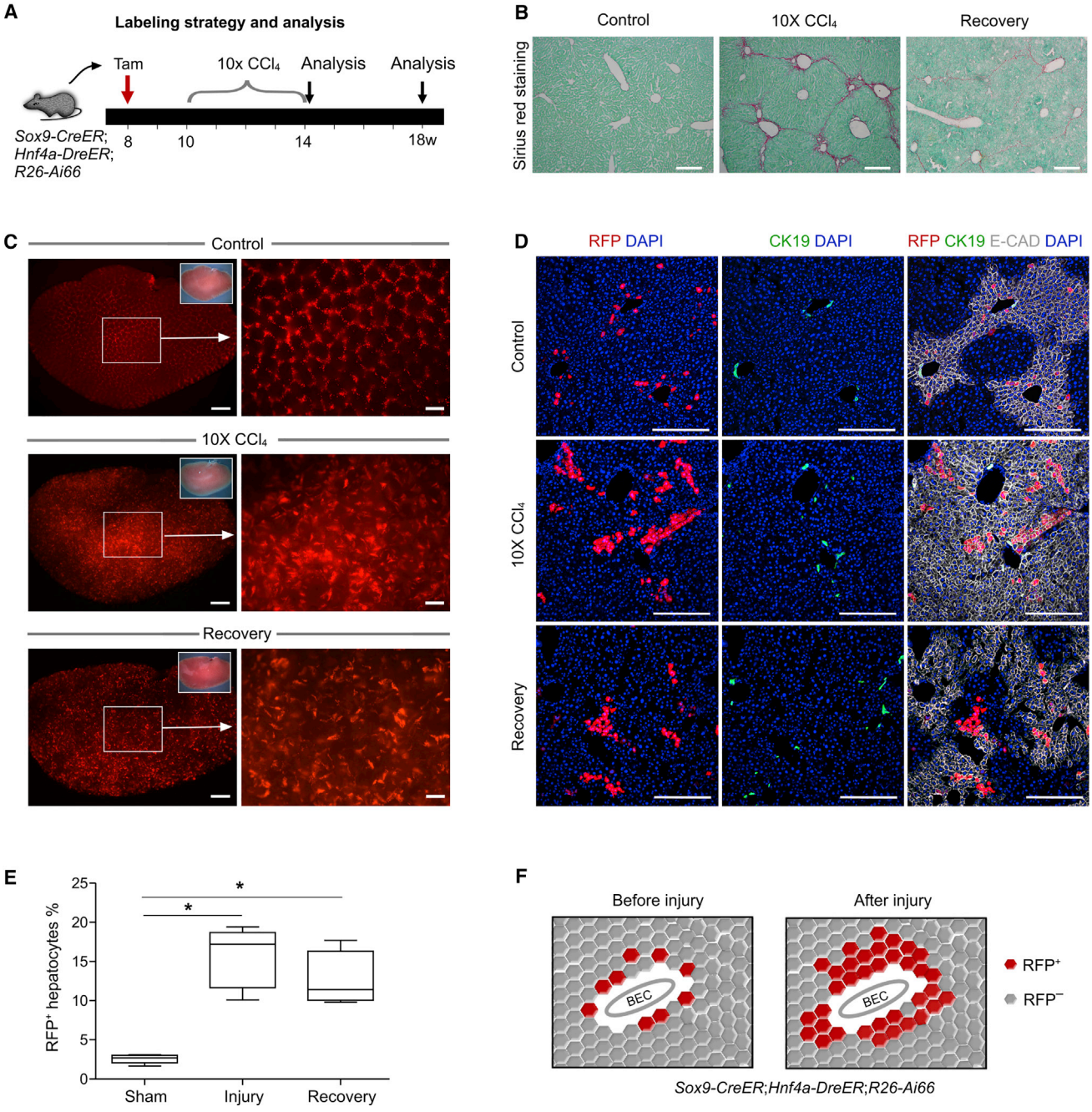

Figure 3. SOX9$^+$ Hepatocytes Contribute Parenchymal Restoration after CCl_4-Induced Liver Damage

(A) Experimental strategy for tamoxifen treatment (Tam) and tissue analysis at different time points after injury.

(B) Sirius red staining of liver sections from oil (Control) or CCl_4-treated mice.

(C) Whole-mount fluorescence view of *Sox9-CreER;Hnf4a-DreER;Rosa26-Ai66* liver after oil (Control) or CCl_4 treatment or recovery.

(D) Immunostaining for RFP, CK19, and E-CAD on liver sections shows the expansion of RFP$^+$ hepatocytes following injuries.

(E) Quantification of RFP$^+$ hepatocytes in control, injury, or recovery groups. Data are mean ± SEM, n = 5; *p < 0.05.

(F) Cartoon image showing expansion of SOX9$^+$ hepatocytes after injury.

Scale bars, 200 μm (B), 1 mm (C, left), 500 μm (C, right), and 100 μm (D).

CCl_4-induced liver injury (Figure 3D). Quantitatively, the percentage of RFP^+ hepatocytes was significantly higher in the injured liver and recovered liver than in the control group (15.22% ± 1.57%, 12.99% ± 1.51%, and 2.55% ± 0.28%, respectively, Figure 3E), indicating expansion of $SOX9^+$ hepatocytes in CCl_4-induced injury (Figure 3F).

We also performed PHx in 10-week-old mice and analyzed liver tissues at 12–14 weeks of age (Figure S2A). Sirius red staining showed that there was no significant tissue fibrosis in the sham or recovery group 2 weeks or 4 weeks after the operation (R2W or R4W, Figure S2B). By whole-mount fluorescent imaging and sectional immunostaining for RFP, we found that $SOX9^+$ hepatocytes did not expand preferentially after PHx compared with $SOX9^-$ hepatocytes (Figures S2C–S2E). By immunostaining with the BEC marker CK19, we found that these $SOX9^+$ hepatocytes did not give rise to BECs after PHx and remained as hepatocytes after injury (Figure S2D). We observed an increase in $Ki67^+$ hepatocytes after PHx injury compared with the sham control (Figure S2F). However, the percentage of RFP^+ hepatocytes did not change significantly, indicating that PHx did not preferentially induce $SOX9^+$ hepatocyte expansion. Thus, $SOX9^+$ hepatocytes are a unique cell population that responds to a certain type of liver injury (such as CCl_4) through significant self-expansion.

$SOX9^+$ Hepatocytes Contribute to Cholangiocytes after Bile Duct Ligation or DDC-Induced Liver Injury

Previous work reported that bile duct ligation (BDL) or 3,5-diethoxycarbonyl-1,4-dihydrocollidine (DDC) treatment induces hepatocytes to transition into BECs (Michalopoulos et al., 2005; Tarlow et al., 2014b). We next examined whether $SOX9^+$ hepatocytes contribute to BECs after BDL- or DDC-induced liver injury. After tamoxifen treatment and a 2-week washout period, *Sox9-CreER;Hnf4a-DreER;R26-Ai66* mice were subjected to BDL at 10 weeks old, and livers were collected at 12 or 14 weeks for analysis (Figure 4A). BDL resulted in significant liver fibrosis compared with the sham group (Figure 4B). In contrast to the CCl_4 treatment, BDL injury did not stimulate significant expansion of $SOX9^+$ hepatocytes (Figure 4C). Notably, a subset of RFP^+ hepatocytes gave rise to BECs in the BDL-injured liver, while RFP^+ BECs were not detected in the sham control group (Figure 4C). Quantitatively, 2.48% ± 0.19% and 0.99% ± 0.28% of hepatocytes were RFP^+ in the sham and injury groups, respectively ($^*p < 0.05$; n = 5) (Figure 4D), indicating that BDL injury significantly reduced the $SOX9^+$ hepatocyte population. The reduction in $SOX9^+$ hepatocytes could be due to the lower competence of $SOX9^+$ hepatocytes in expansion compared with $SOX9^-$ hepatocytes during liver injury. It is also likely that $SOX9^+$ hepatocytes have an enhanced potential to develop into BECs. In the BDL liver, 3.46% ± 0.33% of BECs were RFP^+, indicating that $SOX9^+$ hepatocytes differentiated into BECs after BDL injury (Figures 4E and 4F). Tamoxifen induction in *Alb-CreER;R26-RFP* mice resulted in labeling of almost all hepatocytes (>99%, n = 5), and 10.49% ± 0.59% BECs were RFP^+ in *Alb-CreER;R26-RFP* mouse livers after BDL injury (Figures 4G and 4H). In the liver, almost all hepatocytes contributed to approximately 10% of the BECs after BDL (99% hepatocytes to 10% BECs), while labeled $SOX9^+$ hepatocytes that constituted less than 3% of all hepatocytes gave rise to over 3% of the BECs after BDL (~3% hepatocytes to ~3% BECs). Therefore, compared with the majority of hepatocytes that were negative for SOX9, this $SOX9^+$ hepatocyte population had a greater propensity to differentiate into BECs after BDL.

Alternatively, we also used a DDC-induced cholestatic liver injury model. Two weeks after tamoxifen treatment, mice were treated with DDC and liver samples were collected 8 weeks later (Figure 4I). Compared with the sham group, significant fibrosis was detected in the DDC-treated mouse livers (Figure 4J). Immunostaining for RFP and CK19 identified RFP^+CK19^+ BECs in the DDC-treated liver but not in controls (Figure 4K). Quantitatively, 2.59% ± 0.29% and 1.07% ± 0.14% of hepatocytes were RFP^+ in the sham and DDC-treated livers, respectively ($^*p < 0.05$; n = 5) (Figure 4L). In the DDC group, 3.63% ± 0.27% of BECs were RFP^+, indicating the contribution of $SOX9^+$ hepatocytes to BECs (Figures 4M and 4N). Likewise, we also induced *Alb-CreER;R26-RFP* mice with DDC and found that 11.31% ± 0.68% of BECs were RFP^+ (Figures 4O and 4P). Quantitatively, >99% of hepatocytes labeled by *Alb-CreER* contributed to ~11% of BECs. In comparison, less than 3% of hepatocytes marked by SOX9 contributed to over 3% of BECs, indicating that $SOX9^+$ hepatocytes might have a greater propensity to give rise to BECs after DDC-induced injury. Taken together, these data demonstrated that while the $SOX9^+$ hepatocyte number was reduced, these cells contributed to *de novo* BECs after BDL or DDC injuries.

Generation of and Characterization of the *R26-Confetti2* Mouse Line

The above data indicated that $SOX9^+$ hepatocytes responded distinctly in different injury models. At the population level, $SOX9^+$ cells could adopt both BEC and hepatocyte fates. We next asked whether some hepatocytes were predetermined to generate BECs or had the potential to generate both cell lineages during injury. To address this, we developed a strategy for single-cell clonal analysis of $SOX9^+HNF4a^+$ hepatocytes. The *R26-Confetti* reporter was previously generated to allow more precise clonal fate-mapping studies (Snippert et al., 2010). The conventional *R26-Confetti* is operated based on Cre-loxP recombination

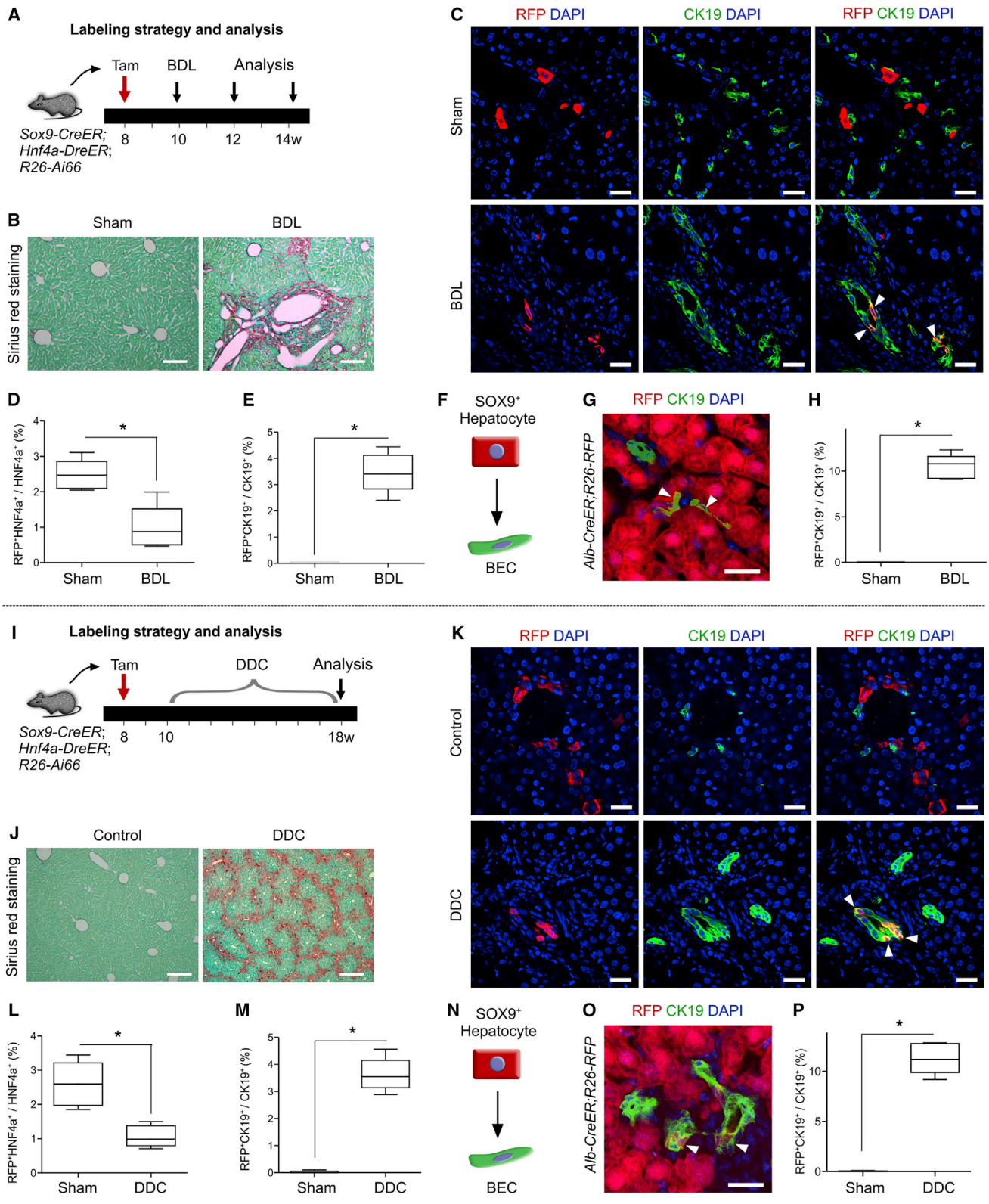

Figure 4. SOX9$^+$ Hepatocytes Contribute to Cholangiocytes after BDL- or DDC-Induced Liver Injury

(A and I) Experimental strategies for tamoxifen treatment (Tam), liver injuries, and tissue analysis.

(B and J) Sirius red staining of liver sections from control and BDL-treated (B) or DDC-treated (J) mice.

(legend continued on next page)

that leads to four different fluorescence readouts, permitting sparse labeling of cells in one color for more rigorous clonal analysis. To specifically label SOX9$^+$HNF4a$^+$ hepatocytes for clonal analysis, we generated a secondary version of *R26-Confetti* (*R26-Confetti2*) that was responsive to two orthogonal recombinases, Cre and Dre. A cDNA containing the CAG-rox-Stop-rox-Confetti cassette was knocked into the Rosa26 gene locus by homologous recombination (Figure 5A). When this *R26-Confetti2* reporter was crossed with Cre and Dre mouse lines, there were distinct fluorescent readouts for cells: Cre$^+$Dre$^-$ cells were negative for any fluorescence; Cre$^-$Dre$^+$ cells were positive for CFP but negative for other types of fluorescence; and Cre$^+$Dre$^+$ cells were positive for three fluorescent proteins, YFP, GFP, and RFP (Figure 5B). We next performed some control experiments to test whether *R26-Confetti2* worked as designed. For *R26-Confetti2* alone, there was no detectable fluorescence signal in the liver (Figure 5C). For *CAG-Dre;R26-Confetti2* mice, cells in the liver expressed CFP in whole-mount or sectional imaging (Figure 5D). CFP, but not other fluorescence signals, was also detected in other organs of *CAG-Dre;R26-Confetti2* mice (Figure S3A). For *CAG-CreER;R26-Confetti2* mice treated with tamoxifen, there was no detectable fluorescence signal in the liver in whole-mount and sectional imaging (Figure 5E). We did not detect fluorescence signals in other organs or tissues (Figure S3B). For *CAG-CreER;CAG-Dre;R26-Confetti2* mice treated with tamoxifen, we could detect CFP, GFP, YFP, and RFP signals in the liver (Figure 5F). Similarly, we detected these fluorescence signals in other organs, such as the heart (Figures S4A and S4B). Taken together, the above data indicated that *R26-Confetti2* functioned as expected and could be used for clonal analysis of single SOX9$^+$HNF4a$^+$ hepatocytes during liver injury.

We used *R26-Confetti2* for the analysis of SOX9$^+$HNF4a$^+$ hepatocytes during liver homeostasis. Mouse crossing generated three different genotypes among mouse littermates: *Hnf4a-DreER;R26-Confetti2*, *Sox9-CreER;R26-Confetti2*, and *Hnf4a-DreER;Sox9-CreER;R26-Confetti2*. For these three groups, we injected tamoxifen at the adult stage (8–10 weeks old) and then collected liver samples for analysis after 10–12 weeks. Sectional imaging of *Hnf4a-DreER;R26-Confetti2* liver tissues showed that hepatocytes were positive for CFP only (Figure 5G). There was no detectable fluorescence signal in *Sox9-CreER;R26-Confetti2* mouse livers (Figure 5H). In *Hnf4a-DreER;Sox9-CreER;R26-Confetti2* mice, Dre-rox recombination led to a subset of HNF4a$^+$ hepatocytes labeled with CFP (arrowheads, Figure 5I). Both Dre-rox and Cre-loxP recombination led to one of the other three fluorescence signals, such as sparse RFP labeling in HNF4a$^+$SOX9$^+$ hepatocytes (arrow, Figure 5I). The sparsely labeled SOX9$^+$ hepatocytes remained as single cells and did not contribute to any ductal cell during liver homeostasis.

Bipotency of Single SOX9$^+$ Hepatocytes after Liver Injury

After labeling sparse SOX9$^+$ hepatocytes after tamoxifen treatment, *Hnf4a-DreER;Sox9-CreER;R26-Confetti2* mice were subjected to DDC-induced liver injury, and liver tissues were collected for analysis after 8–10 weeks. We observed very sparse labeling in the injured liver, and cell labeling could be categorized into three distinct clones: hepatocytes, BECs, and mixed clones that contained both hepatocytes and BECs (Figures 6A and 6B). Two or three labeled hepatocytes, such as nGFP$^+$ or YFP$^+$ hepatocytes, were detected (Figures 6A and 6B), indicating cell proliferation after liver injury. To determine whether some of the labeled SOX9$^+$ hepatocytes generated BECs after injury, we stained the liver sections with CK19 and developed the signal in the far-red channel to avoid mixing with other fluorescence signals. In each field there was only one clone with a unique fluorescent color, such as GFP, YFP, or RFP. We found that a substantial number of clones exhibited CK19 expression, indicating that they were the BEC clones (arrowheads, Figures 6A and 6B). Fewer clones were hepatocytes in the injured liver, and these labeled hepatocytes in one clone were usually detected in a cluster (arrows, Figures 6A and 6B), indicating their proliferation after injury. Interestingly, we also detected mixed clones that contained both hepatocytes and BECs in one single-color clone (Figures 6A and 6B), suggesting that these two different cell lineages could be derived from a single SOX9$^+$ hepatocyte. We next collected serial liver sections and stained them with CK19 for analysis of all the labeled cells in each clone

(C and K) Immunostaining for RFP and CK19 on liver sections shows that SOX9$^+$ hepatocytes contribute to BECs (arrowheads) following BDL-induced (C) or DDC-induced (K) liver injury.
(D and L) Quantification of the RFP$^+$ hepatocytes percentage. *$p < 0.05$ ($n = 5$).
(E and M) Quantification of RFP$^+$ BECs percentage. *$p < 0.05$ ($n = 5$).
(F and N) Cartoon images showing contribution of SOX9$^+$ hepatocyte to BEC (arrowheads) after BDL-induced (F) or DDC-induced (N) liver injury.
(G and O) Immunostaining for RFP and CK19 on liver sections collected from *Alb-CreER;R26-RFP* after BDL-induced (G) or DDC-induced (O) injury.
(H and P) Quantification of RFP$^+$ BECs percentage. *$p < 0.05$ ($n = 5$).
Scale bars, 200 μm (B and J) and 50 μm (C, G, K, and O).

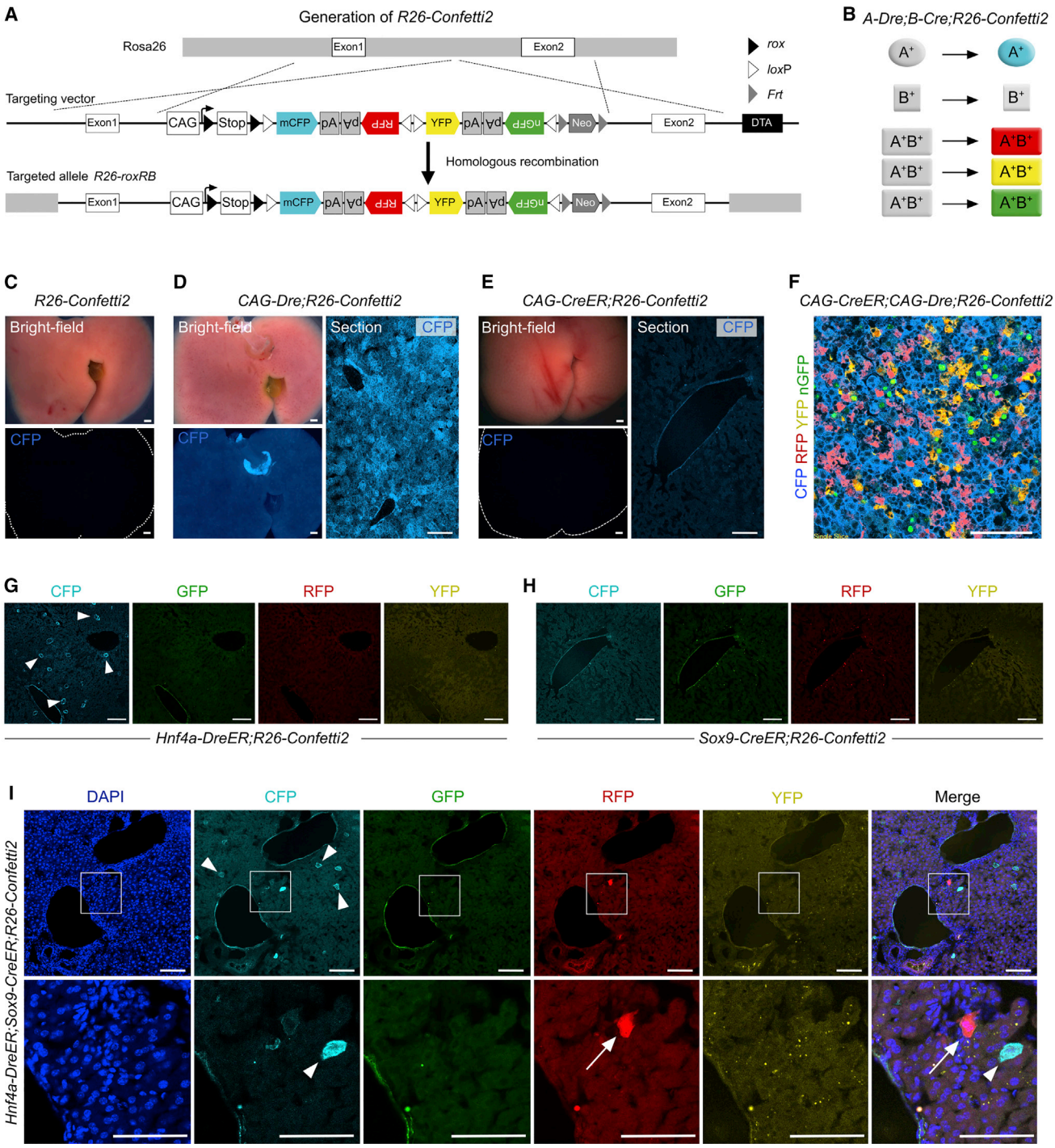

Figure 5. Generation and Characterization of *R26-Confetti2* Mouse

(A) Schematic showing strategy for generation of *R26-Confetti2* reporter allele by homologous recombination.

(B) Distinct cell labeling after Cre and Dre recombinations.

(C–E) Whole-mount fluorescent images of *R26-Confetti2* (C), *CAG-Dre;R26-Confetti2* (D), and *CAG-CreER;R26-Confetti2* (E) mouse livers. CFP is detected in *CAG-Dre;R26-Confetti2* liver and its section, but not in *R26-Confetti2* or *CAG-CreER;R26-Confetti2* livers. Tamoxifen was induced 2 days before tissue collection.

(F) Fluorescent image of liver section from *CAG-CreER;CAG-Dre;R26-Confetti2* mouse. Tamoxifen was induced at 12.5 days before tissue collection.

(legend continued on next page)

(Figure 6C). Serially stained sections showed the clone clearly in the liver and confirmed the bipotency of a single SOX9$^+$ hepatocyte during liver injury (Figures 6C, S5, and S6). Quantification of the three types of clones in *Hnf4a-DreER;Sox9-CreER;R26-Confetti2* livers after injury showed hepatocyte clones, BEC clones, and mixed clones that constituted 35.32% ± 0.82%, 55.54% ± 2.10%, and 9.13% ± 1.91% of all clones, respectively (Figure 6D). We also quantified the cell number of each clone and found that there were 4.73 ± 0.39 hepatocytes in hepatocyte clones; 6.03 ± 0.41 BECs in BEC clones; and 2.87 ± 0.20 hepatocytes and 6.78 ± 0.42 BECs in mixed clones (Figure 6E). We confirmed the bipotency of SOX9$^+$ hepatocytes by clonal analysis in the BDL model (Figure S7). Thus, clonal fate-mapping analysis of a single SOX9$^+$ hepatocyte showed their uni- and bipotency during liver injury and repair (Figure 6F).

DISCUSSION

Two major epithelial cell populations, BECs and hepatocytes, have recently been reported to give rise to each other under specific injury or disease conditions (Deng et al., 2018; Raven et al., 2017; Schaub et al., 2018; Tarlow et al., 2014b; Yanger et al., 2013, 2014). Whether a single hepatocyte is bipotent for both BECs and hepatocytes remains unknown. A recent study reported that SOX9$^+$ hepatocytes exhibit a high proliferative potential depending on the condition of injury without tumorigenesis (Font-Burgada et al., 2015). In our study, we used a dual recombinase-based lineage-tracing strategy to genetically target SOX9$^+$ hepatocytes. We found that a single SOX9$^+$ hepatocyte differentiated into both BECs and hepatocytes after injury, providing genetic evidence for the existence of bipotent SOX9$^+$ hepatocytes as progenitor cells for liver repair and regeneration.

This work mainly utilized genetic tools to specifically label SOX9$^+$ hepatocytes. The combination of Cre-loxP and Dre-rox allowed another layer of regulation in the specificity in genetic targeting. Our recent study using dual recombinases and a nested reporter (*NR1*) permitted specific labeling of SOX9$^+$ BECs without contamination of SOX9$^+$ hepatocytes (He et al., 2017). Unlike a previous study reporting the differentiation of SOX9$^+$ ductal cells to hepatocytes (Furuyama et al., 2011), our fate mapping of SOX9$^+$ BECs showed their ductal cell fate but not hepatocyte fate via differentiation during liver homeostasis or after injury (He et al., 2017). The proposed ductal cell-specific *Sox9-CreER* used in a previous study (Furuyama et al., 2011) might not be specific for ductal cells, as SOX9 is also expressed in hepatocytes (Figures 1C and 1G), although the expression level of SOX9 in hepatocytes is lower than that that of BECs. As *Sox9-CreER* labels hepatocytes in addition to BECs, the contribution of SOX9$^+$ progenitors to hepatocytes (Furuyama et al., 2011) could also be interpreted to indicate that SOX9$^+$ hepatocytes labeled at the beginning contributed to more hepatocytes during liver regeneration after injury. Genetic lineage tracing with "duct-specific" Cre stains should be carefully examined to determine whether any hepatocyte was labeled.

With the advent of single-cell sequencing technology, more different subsets of hepatocytes (Halpern et al., 2017) or biliary epithelial cell populations (Tarlow et al., 2014b) could be elucidated, and their *in vivo* functions remain largely unknown. Our dual recombinase-mediated genetic systems reported here would be valuable to more precisely label a subset of liver cell populations and study their cell fate during liver homeostasis and injuries. Moreover, we recently developed a sequential intersectional genetics strategy whereby Dre-rox recombination mediates the release of Cre (Pu et al., 2018). This strategy would also allow gene functional analysis by crossing the Dre-mediated Cre mouse strain with the available flox gene allele for *in vivo* gain- or loss-of-function studies. Moreover, dual recombination systems could be used to manipulate two distinct cell populations *in vivo* to understand their function and cell plasticity during liver injuries.

SOX9 has been previously studied as a progenitor or stem cell marker for cell expansion and fate determination (Guo et al., 2012; Lincoln et al., 2007; Zhang et al., 2017). During injury, SOX9 could also be activated in hepatocytes (Cao et al., 2017; He et al., 2014). SOX9$^+$ hepatocytes are located near ductal cells and could contribute to BECs during liver injuries (Yanger et al., 2013). These SOX9$^+$ hepatocytes, compared with the remaining SOX9$^-$ hepatocytes, have a propensity to contribute to BECs after injuries. Quantitatively, the contribution of SOX9$^+$ hepatocytes to BECs was 10-fold more efficient than SOX9$^-$ hepatocytes after BDL- or DDC-induced liver injuries. SOX9 may predispose hepatocytes to conditions that facilitate reprogramming into BECs (Yanger et al., 2013). Signaling pathways that regulate hepatocytes to BECs include Notch (Fan et al., 2012; Sekiya and Suzuki, 2012), Hippo-Yap (Yimlamai

(G and H) Fluorescent images of liver sections from *Hnf4a-DreER;R26-Confetti2* (G) or *Sox9-CreER;R26-Confetti2* (H) mouse. There are no GFP, RF,P or YFP signals detected in liver sections.

(I) Fluorescent image of *Hnf4a-DreER;Sox9-CreER;R26-Confetti2* mouse liver sections. Arrows indicate sparse RFP$^+$ hepatocytes, and arrowheads indicate hepatocytes that have recombined with DreER but not CreER.

Each image is representative of five individual samples. Scale bars, 100 μm.

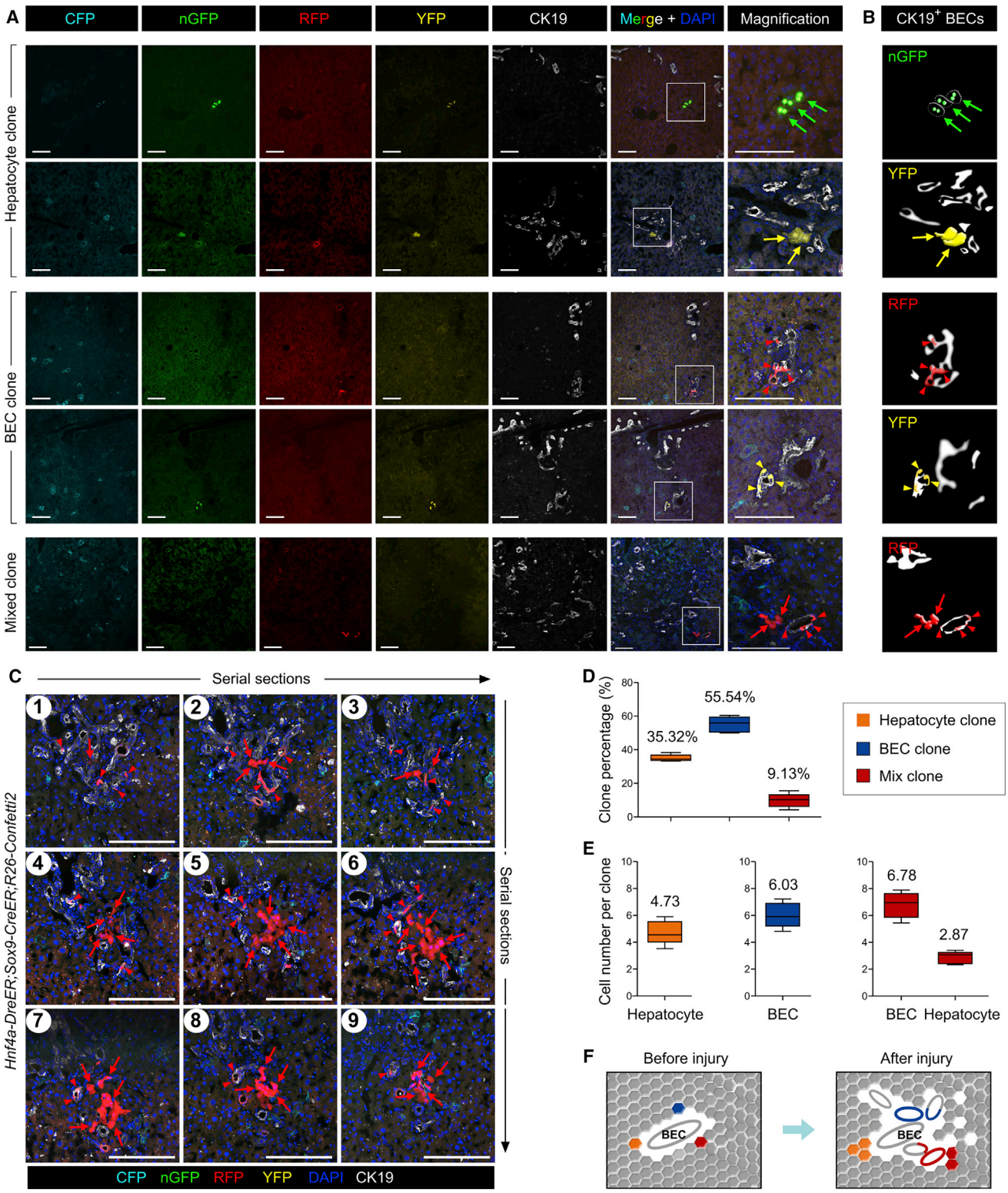

Figure 6. Identification of Bipotent SOX9$^+$ Hepatocyte after Liver Injury

(A and B) Fluorescent sections stained with BEC marker CK19 shows three distinct clones: hepatocyte clone, BEC clone, and mixed clone that contains both hepatocyte and BEC. Arrows or arrowheads indicate nGFP$^+$, RFP$^+$, or YFP$^+$ hepatocytes or BECs, respectively. Cartoon images in (B) denote the magnified images in (A).

(legend continued on next page)

et al., 2014), and TGFβ (Schaub et al., 2018). Whether these signaling pathways were activated in SOX9$^+$ hepatocytes to modulate their bipotency after liver injury merits investigation in the future. Alternatively, the adjacent ductal cells could directly or indirectly affect and reprogram the cell fate of SOX9$^+$ hepatocytes. Whether ductal cells influence the cell fate of hepatocytes through paracrine signaling remains unknown, and niche signaling has now been reported to influence the function of cells rather than the hard-wired property of stem cells (Clevers and Watt, 2018). It is therefore of interest whether these SOX9$^+$ hepatocytes, relocated away from the portal region, could maintain the robust ability to differentiate into BECs. Elucidation of the regulatory mechanism of SOX9$^+$ hepatocyte progenitors may provide information for amplifying the bipotent progenitor population for potential applications in liver repair and regeneration. As SOX9$^+$ hepatocytes are unique in their ability to differentiate into BECs and expand hepatocytes, they could be a potentially important drug target for treating liver diseases in the future.

EXPERIMENTAL PROCEDURES

Mice

All mouse studies were carried out strictly according to the guidelines of the Institutional Animal Care and Use Committee at the Institute of Biochemistry and Cell Biology and the Institute for Nutritional Sciences, Shanghai Institutes for Biological Sciences, Chinese Academy of Sciences. *Hnf4a-DreER* was generated by CRISPR/Cas9 through homologous recombination. A complementary cDNA encoding IRES-DreER^{T2} was inserted in-frame with the translation codon of the *Hnf4a* gene. The chimeric mice positive for targeted ESCs were germline transferred to F1 generation and bred on a C57BL/6 × ICR background. The *Sox9-CreER^{T2}* line was generated by the National Institute for Biological Sciences, Beijing, China. *R26-Ai66* (*Rosa26-rox-Stop-rox-loxP-Stop-loxP-tdTomato*) was generated as reported previously (Madisen et al., 2015; Zhang et al., 2016). The *Rosa26-Rox-Stop-Rox-tdTomato* (*R26-RSR-RFP*) mouse line was generated by crossing *ACTB-Cre* with *R26-Ai66* to excise the second loxP-flanked Stop cassette, and *ACTB-Cre* was not passaged to the subsequent mouse breeding. *R26-RSR-RFP* was responsive to Dre but not Cre recombinase. The *Rosa26-rox-Stop-rox-Confetti* (*R26-Confetti2*) was generated by targeting CAG-rox-Stop-rox-Confetti cassette into the Rosa26 gene locus by homologous recombination (Figure 5A). All experimental mice were maintained on a C57BL6/ICR mixed background. Tamoxifen (Sigma, T5648) was dissolved in corn oil (20 mg/mL) and administered by gavage at the indicated time points. We treated *R26-RFP* and *R26-Confetti2* mice with 0.4 mg of tamoxifen per gram of mouse body weight (mg/g) and 0.15 mg/g tamoxifen, respectively.

Genomic PCR

Genomic DNA was prepared from mouse tails according to the standard protocols described previously (Wang et al., 2017). All mice were genotyped with specific primers that distinguish knockin allele from wild-type allele. Information on the primers can be found in Supplemental Information.

Injury Model

For the CCl_4-induced chronic injury model, CCl_4 was dissolved at 1:3 in corn oil and injected intraperitoneally at a dose of 4 μL/g body weight every 3 days, repeated 10 times. Partial hepatectomy (PHx) was generated by removing two-thirds of the liver to induce the injury (Wang et al., 2017). The BDL injury model was prepared according to established protocols described previously (Pu et al., 2016). For the DDC-induced chronic injury model, mice received mouse diet (Harlan Teklad, 5015) containing 0.1% DDC (Sigma-Aldrich).

Whole-Mount Fluorescence Microscopy

Collected mouse liver was washed in PBS and placed on agar for the whole-mount bright-field and fluorescence imaging using a Zeiss stereoscope (AxioZoom V16). To determine magnification of specific regions, we used the automated z-stack images acquired by the stereoscope (Zeiss AxioZoom V16).

Immunostaining

Immunostaining was performed according to the standard protocols described previously (Tian et al., 2013). The following antibodies were used: RFP (Rockland, 600-401-379, 1:200), HNF4a (Santa Cruz Biotechnology, sc-6556, 1:100), cytokeratin 19 (CK19, Developmental Studies Hybridoma Bank, TROMA-III, 1:100), VE-cadherin (R&D Systems, AF1002, 1:100), desmin (R&D, AF3844, 1:100), PDGFRα (R&D, AF1062, 1:100), E-cadherin (Cell Signaling Technology, 3195, 1:100), EpCAM (Abcam, ab92383, 1:100), αSMA (Sigma, F3777, 1:100), and Ki67 (Thermo Scientific, RM-9106-S0, 1:100). Signals were developed with Alexa fluorescence antibodies (Invitrogen), and nuclei were counterstained with 4′,6-diamidino-2-phenylindole (Vector Laboratories). For clonal analysis, CK19 was stained on the liver sections in the far-red channel. In total 246 clones were analyzed: 820 cholangiocytes in cholangiocyte clones; 412 hepatocytes in hepatocyte clones; 156 cholangiocytes; and 66 hepatocytes in mixed clones. There was bleed-through of fluorescence for YFP and GFP because the YFP signal could also be detected in the GFP channel. In

(C) Serial sections of a bipotent clone that contains both BECs (arrowheads) and hepatocytes (arrows).
(D) Quantification of the percentage of three types of clones in injured liver. A total of 246 clones were analyzed. Data are mean ± SEM; n = 5.
(E) Quantification of cell number in each type of clones. A total of 246 clones were analyzed. Data are mean ± SEM; n = 5.
(F) Cartoon figure showing the cell fate of three types of clones after injury.
Scale bars, 100 μm.

addition, our GFP is nGFP (nuclear), so the pure GFP signal should be in the nucleus while the bleed-through signal in the GFP channel from YFP should not be a nuclear signal. Immunostaining images were acquired by an Olympus fluorescence microscope (BX53), a Zeiss stereomicroscope (AxioZoom V16), a Zeiss confocal laser scanning microscope (LSM510), and an Olympus confocal microscope (FV1200).

Sirius Red Staining

Sirius red staining was used to assess fibrotic tissue in chronic injury models, and was performed according to the standard protocols described previously (Wang et al., 2017).

Statistics

All data were collected from at least five independent experiments as indicated. Data for two groups were analyzed by a two-sided unpaired Student's t test, whereas comparison between more than two groups was performed using an analysis of variance followed by Tukey's multiple comparison tests. Significance was accepted when $p < 0.05$. All data are presented as mean values ± SEM.

ACCESSION NUMBERS

Data supporting the findings of this study are available within the article and its Supplemental Information, and from the corresponding author upon reasonable request.

SUPPLEMENTAL INFORMATION

Supplemental Information includes Supplemental Experimental Procedures and seven figures and can be found with this article online at https://doi.org/10.1016/j.stemcr.2019.01.010.

AUTHOR CONTRIBUTIONS

X. Han, Y.W., J.L., and B.Z. designed the study. X. Han and Y.W. performed experiments and analyzed the data. W.P., X. Huang, L.Q., Y.L., W.Y., H.Z., X.L., L.H., and L.Z. bred the mice, performed experiments, or provided material and valuable comments. Y.J., J.L., and K.O.L. provided reagents and intellectual input to this study and edited the manuscript. B.Z. supervised the study, analyzed the data, and wrote the manuscript.

ACKNOWLEDGMENTS

We thank Shanghai Model Organisms Center for mouse generation; and Baojin Wu, Guoyuan Chen, Zhonghui Weng, and Aimin Huang for animal husbandry. We also thank the technical help from Wei Bian, Tengfei Zhang, and members of National Center for Protein Science Shanghai for assistance in microscopy. This work was supported by the Strategic Priority Research Program of the Chinese Academy of Sciences (CAS, XDA16020204, XDB19000000), National Key Research & Development Program of China (2018YFA0107900, 2018YFA0108100, 2016YFC1300600, 2017YFC1001303), National Science Foundation of China (31730112, 91639302, 31625019, 91849202, 81761138040, 81872241, 31701292), Youth Innovation Promotion Association of CAS (2060299), Key Project of Frontier Sciences of CAS (QYZDB-SSW-SMC003), Shanghai Science and Technology Commission (17ZR1449600), the Program for Guangdong Introduction Innovative and Enterpreneurial Teams (2017ZT07S347), Shanghai Yangfan Project, China Postdoctoral Science Foundation, China Postdoctoral Innovative Talent Support Program, China Young Talents Lift Engineering, Boehringer Ingelheim, Sanofi-SIBS Fellowship, AstraZeneca, Royal Society-Newton Advanced Fellowship, Research Council of Hong Kong (04110515, 14111916, C4024-16W), and Health and Medical Research Fund (03140346, 04152566).

Received: October 14, 2018
Revised: January 14, 2019
Accepted: January 16, 2019
Published: February 14, 2019

REFERENCES

Antoniou, A., Raynaud, P., Cordi, S., Zong, Y., Tronche, F., Stanger, B.Z., Jacquemin, P., Pierreux, C.E., Clotman, F., and Lemaigre, F.P. (2009). Intrahepatic bile ducts develop according to a new mode of tubulogenesis regulated by the transcription factor SOX9. Gastroenterology *136*, 2325–2333.

Cao, W., Chen, K., Bolkestein, M., Yin, Y., Verstegen, M.M.A., Bijvelds, M.J.C., Wang, W., Tuysuz, N., Ten Berge, D., Sprengers, D., et al. (2017). Dynamics of proliferative and quiescent stem cells in liver homeostasis and injury. Gastroenterology *153*, 1133–1147.

Clevers, H., and Watt, F.M. (2018). Defining adult stem cells by function, not by phenotype. Annu. Rev. Biochem. *87*, 1015–1027.

Deng, X., Zhang, X., Li, W., Feng, R.X., Li, L., Yi, G.R., Zhang, X.N., Yin, C., Yu, H.Y., Zhang, J.P., et al. (2018). Chronic liver injury induces conversion of biliary epithelial cells into hepatocytes. Cell Stem Cell *23*, 114–122.e3.

Espanol-Suner, R., Carpentier, R., Van Hul, N., Legry, V., Achouri, Y., Cordi, S., Jacquemin, P., Lemaigre, F., and Leclercq, I.A. (2012). Liver progenitor cells yield functional hepatocytes in response to chronic liver injury in mice. Gastroenterology *143*, 1564–1575.e7.

Fan, B., Malato, Y., Calvisi, D.F., Naqvi, S., Razumilava, N., Ribback, S., Gores, G.J., Dombrowski, F., Evert, M., Chen, X., and Willenbring, H. (2012). Cholangiocarcinomas can originate from hepatocytes in mice. J. Clin. Invest. *122*, 2911–2915.

Farber, E. (1956). Similarities in the sequence of early histological changes induced in the liver of the rat by ethionine, 2-acetylamino-fluorene, and 3′-methyl-4-dimethylaminoazobenzene. Cancer Res. *16*, 142–148.

Font-Burgada, J., Shalapour, S., Ramaswamy, S., Hsueh, B., Rossell, D., Umemura, A., Taniguchi, K., Nakagawa, H., Valasek, M.A., Ye, L., et al. (2015). Hybrid periportal hepatocytes regenerate the injured liver without giving rise to cancer. Cell *162*, 766–779.

Furuyama, K., Kawaguchi, Y., Akiyama, H., Horiguchi, M., Kodama, S., Kuhara, T., Hosokawa, S., Elbahrawy, A., Soeda, T., Koizumi, M., et al. (2011). Continuous cell supply from a Sox9-expressing progenitor zone in adult liver, exocrine pancreas and intestine. Nat. Genet. *43*, 34–41.

Grompe, M. (2014). Liver stem cells, where art thou? Cell Stem Cell *15*, 257–258.

Guo, W., Keckesova, Z., Donaher, J.L., Shibue, T., Tischler, V., Reinhardt, F., Itzkovitz, S., Noske, A., Zürrer-Härdi, U., Bell, G., et al. (2012). Slug and Sox9 cooperatively determine the mammary stem cell state. Cell *148*, 1015–1028.

Halpern, K.B., Shenhav, R., Matcovitch-Natan, O., Tóth, B., Lemze, D., Golan, M., Massasa, E.E., Baydatch, S., Landen, S., Moor, A.E., et al. (2017). Single-cell spatial reconstruction reveals global division of labour in the mammalian liver. Nature *542*, 352–356.

He, J., Lu, H., Zou, Q., and Luo, L. (2014). Regeneration of liver after extreme hepatocyte loss occurs mainly via biliary transdifferentiation in zebrafish. Gastroenterology *146*, 789–800.e8.

He, L., Li, Y., Li, Y., Pu, W., Huang, X., Tian, X., Wang, Y., Zhang, H., Liu, Q., Zhang, L., et al. (2017). Enhancing the precision of genetic lineage tracing using dual recombinases. Nat. Med. *23*, 1488–1498.

Lincoln, J., Kist, R., Scherer, G., and Yutzey, K.E. (2007). Sox9 is required for precursor cell expansion and extracellular matrix organization during mouse heart valve development. Dev. Biol. *305*, 120–132.

Lu, W.Y., Bird, T.G., Boulter, L., Tsuchiya, A., Cole, A.M., Hay, T., Guest, R.V., Wojtacha, D., Man, T.Y., Mackinnon, A., et al. (2015). Hepatic progenitor cells of biliary origin with liver repopulation capacity. Nat. Cell Biol. *17*, 971–983.

Madisen, L., Garner, A., Shimaoka, D., Chuong, A., Klapoetke, N., Li, L., van der Bourg, A., Niino, Y., Egolf, L., Monetti, C., et al. (2015). Transgenic mice for intersectional targeting of neural sensors and effectors with high specificity and performance. Neuron *85*, 942–958.

Malato, Y., Naqvi, S., Schurmann, N., Ng, R., Wang, B., Zape, J., Kay, M.A., Grimm, D., and Willenbring, H. (2011). Fate tracing of mature hepatocytes in mouse liver homeostasis and regeneration. J. Clin. Invest. *121*, 4850–4860.

Miyajima, A., Tanaka, M., and Itoh, T. (2014). Stem/progenitor cells in liver development, homeostasis, regeneration, and reprogramming. Cell Stem Cell *14*, 561–574.

Michalopoulos, G.K., Barua, L., and Bowen, W.C. (2005). Transdifferentiation of rat hepatocytes into biliary cells after bile duct ligation and toxic biliary injury. Hepatology *41*, 535–544.

Popper, H., Kent, G., and Stern, R. (1957). Ductular cell reaction in the liver in hepatic injury. J. Mt. Sinai Hosp. N. Y. *24*, 551–556.

Pu, W., He, L., Han, X., Tian, X., Li, Y., Zhang, H., Liu, Q., Huang, X., Zhang, L., Wang, Q.D., et al. (2018). Genetic targeting of organ-specific blood vessels. Circ. Res. *123*, 86–99.

Pu, W., Zhang, H., Huang, X., Tian, X., He, L., Wang, Y., Zhang, L., Liu, Q., Li, Y., Li, Y., et al. (2016). Mfsd2a+ hepatocytes repopulate the liver during injury and regeneration. Nat. Commun. *7*, 13369.

Raven, A., Lu, W.Y., Man, T.Y., Ferreira-Gonzalez, S., O'Duibhir, E., Dwyer, B.J., Thomson, J.P., Meehan, R.R., Bogorad, R., Koteliansky, V., et al. (2017). Cholangiocytes act as facultative liver stem cells during impaired hepatocyte regeneration. Nature *547*, 350–354.

Rodrigo-Torres, D., Affo, S., Coll, M., Morales-Ibanez, O., Millan, C., Blaya, D., Alvarez-Guaita, A., Rentero, C., Lozano, J.J., Maestro, M.A., et al. (2014). The biliary epithelium gives rise to liver progenitor cells. Hepatology *60*, 1367–1377.

Schaub, J.R., Huppert, K.A., Kurial, S.N.T., Hsu, B.Y., Cast, A.E., Donnelly, B., Karns, R.A., Chen, F., Rezvani, M., Luu, H.Y., et al. (2018). De novo formation of the biliary system by TGFβ-mediated hepatocyte transdifferentiation. Nature *557*, 247–251.

Schaub, J.R., Malato, Y., Gormond, C., and Willenbring, H. (2014). Evidence against a stem cell origin of new hepatocytes in a common mouse model of chronic liver injury. Cell Rep. *8*, 933–939.

Sekiya, S., and Suzuki, A. (2012). Intrahepatic cholangiocarcinoma can arise from Notch-mediated conversion of hepatocytes. J. Clin. Invest. *122*, 3914–3918.

Snippert, H.J., van der Flier, L.G., Sato, T., van Es, J.H., van den Born, M., Kroon-Veenboer, C., Barker, N., Klein, A.M., van Rheenen, J., Simons, B.D., et al. (2010). Intestinal crypt homeostasis results from neutral competition between symmetrically dividing Lgr5 stem cells. Cell *143*, 134–144.

Suzuki, H., Kanai-Azuma, M., and Kanai, Y. (2015). From sex determination to initial folliculogenesis in mammalian ovaries: morphogenetic waves along the anteroposterior and dorsoventral axes. Sex. Dev. *9*, 190–204.

Tarlow, B.D., Finegold, M.J., and Grompe, M. (2014a). Clonal tracing of SOX9+ liver progenitors in mouse oval cell injury. Hepatology *60*, 278–289.

Tarlow, B.D., Pelz, C., Naugler, W.E., Wakefield, L., Wilson, E.M., Finegold, M.J., and Grompe, M. (2014b). Bipotential adult liver progenitors are derived from chronically injured mature hepatocytes. Cell Stem Cell *15*, 605–618.

Tian, X., Hu, T., Zhang, H., He, L., Huang, X., Liu, Q., Yu, W., He, L., Yang, Z., Zhang, Z., et al. (2013). Subepicardial endothelial cells invade the embryonic ventricle wall to form coronary arteries. Cell Res. *23*, 1075–1090.

Tian, X., Pu, W.T., and Zhou, B. (2015). Cellular origin and developmental program of coronary angiogenesis. Circ. Res. *116*, 515–530.

Wang, Y., Huang, X., He, L., Pu, W., Li, Y., Liu, Q., Li, Y., Zhang, L., Yu, W., Zhao, H., et al. (2017b). Genetic tracing of hepatocytes in liver homeostasis, injury, and regeneration. J. Biol. Chem. *292*, 8594–8604.

Yanger, K., Knigin, D., Zong, Y., Maggs, L., Gu, G., Akiyama, H., Pikarsky, E., and Stanger, B.Z. (2014). Adult hepatocytes are generated by self-duplication rather than stem cell differentiation. Cell Stem Cell *15*, 340–349.

Yanger, K., Zong, Y., Maggs, L.R., Shapira, S.N., Maddipati, R., Aiello, N.M., Thung, S.N., Wells, R.G., Greenbaum, L.E., and Stanger, B.Z. (2013). Robust cellular reprogramming occurs spontaneously during liver regeneration. Genes Dev. *27*, 719–724.

Yimlamai, D., Christodoulou, C., Galli, G.G., Yanger, K., Pepe-Mooney, B., Gurung, B., Shrestha, K., Cahan, P., Stanger, B.Z., and Camargo, F.D. (2014). Hippo pathway activity influences liver cell fate. Cell *157*, 1324–1338.

Zhang, H., Huang, X., Liu, K., Tang, J., He, L., Pu, W., Liu, Q., Li, Y., Tian, X., Wang, Y., et al. (2017). Fibroblasts in an endocardial fibroelastosis disease model mainly originate from mesenchymal derivatives of epicardium. Cell Res. *27*, 1157–1177.

Zhang, H., Pu, W., Tian, X., Huang, X., He, L., Liu, Q., Li, Y., Zhang, L., He, L., Liu, K., et al. (2016). Genetic lineage tracing identifies endocardial origin of liver vasculature. Nat. Genet. *48*, 537–543.

Stem Cell Reports, Volume *12*

Supplemental Information

Lineage Tracing Reveals the Bipotency of SOX9^{+} Hepatocytes during Liver Regeneration

Ximeng Han, Yue Wang, Wenjuan Pu, Xiuzhen Huang, Lin Qiu, Yan Li, Wei Yu, Huan Zhao, Xiuxiu Liu, Lingjuan He, Libo Zhang, Yong Ji, Jie Lu, Kathy O. Lui, and Bin Zhou

SUPPLEMENTAL FIGURES AND LEGENDS

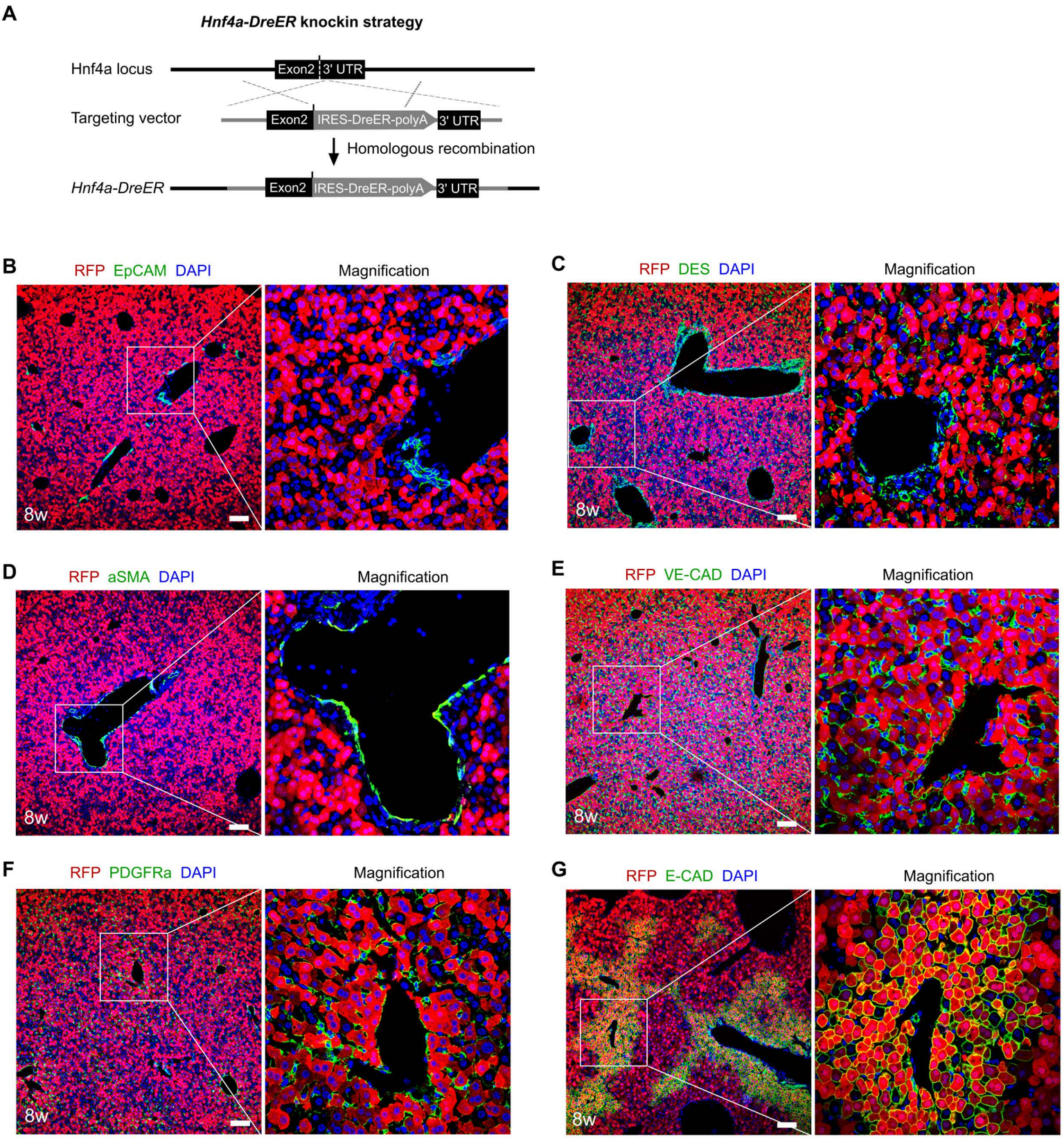

Figure S1: *Hnf4a-DreER* specifically label hepatocytes but not other lineages in adult liver, related to Figure 1
(A) Schematic figure showing knockin strategy for generation of *Hnf4a-DreER* allele.
(B-G) Immunostaining for RFP, EpCAM, DES, aSMA, VE-CAD, PDGFRa and E-CAD on liver sections. Scale bars, 100 μm. Each image is representative of 5 individual samples.

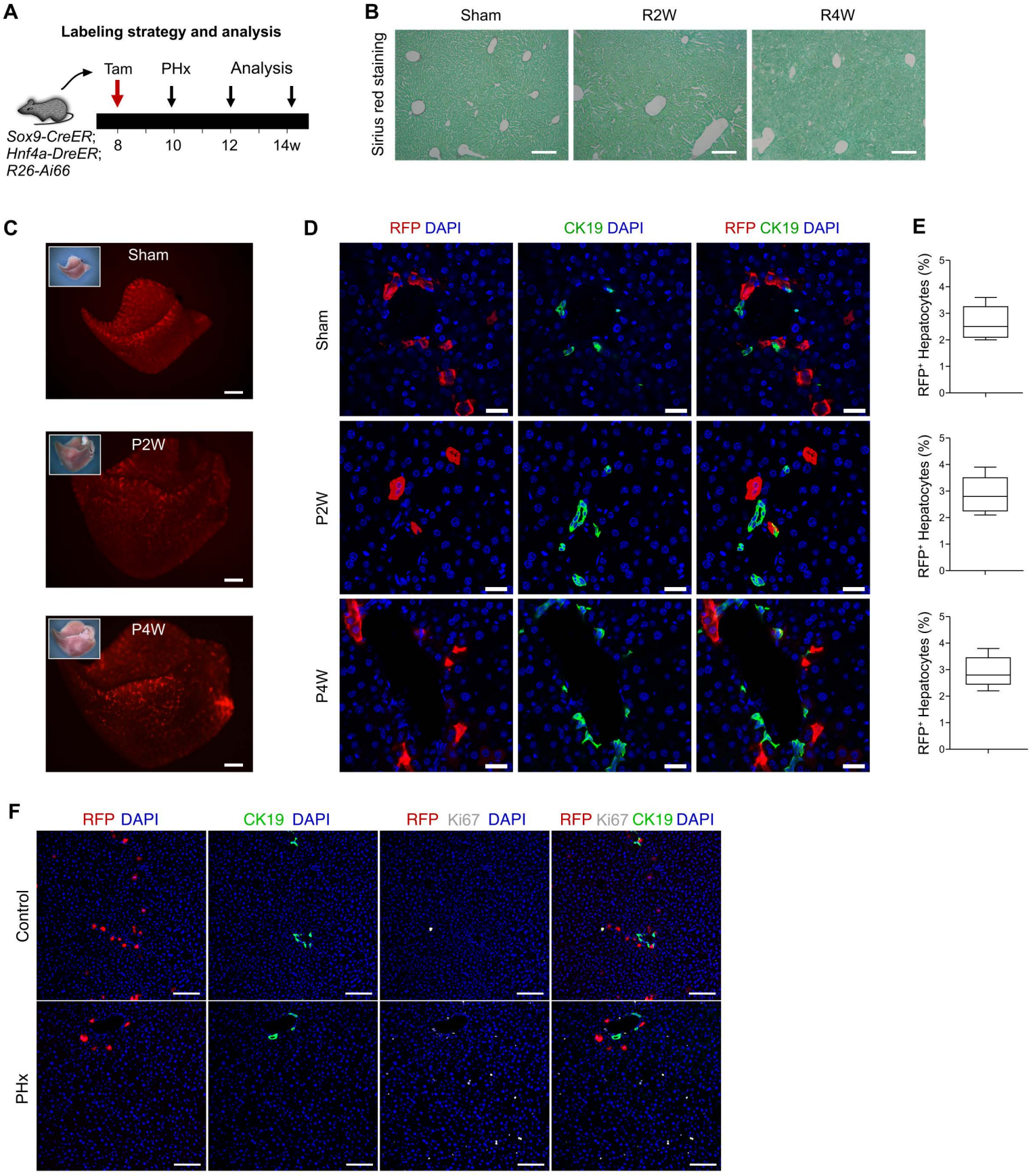

Figure S2: The percentage of RFP⁺ hepatocytes remained unchanged following partial hepatectomy (PHx), related to Figure 3
(**A**) Experimental strategy for tamoxifen treatment (Tam) and tissue analysis at different time points after PHx.
(**B**) Sirius red staining of liver sections from Sham or PHx-injured mice.
(**C**) Whole-mount fluorescence view of *Sox9-CreER;Hnf4a-DreER;R26-Ai66* livers. Inserts are bright-field images.
(**D**) Immunostaining for RFP and CK19 on liver sections shows no change of RFP⁺ cells following PHx injury.
(**E**) Quantification of the percentage of hepatocytes expressing RFP in the liver after PHx injury.
(**F**) Immunostaining for RFP, CK19 and Ki67 on liver sections of PHx or control groups. Scale bars, 200 μm in (**B**); 1 mm in (**C**); 50 μm in (**D**); 100 μm in (**F**). Each image is representative of 5 individual biological samples.

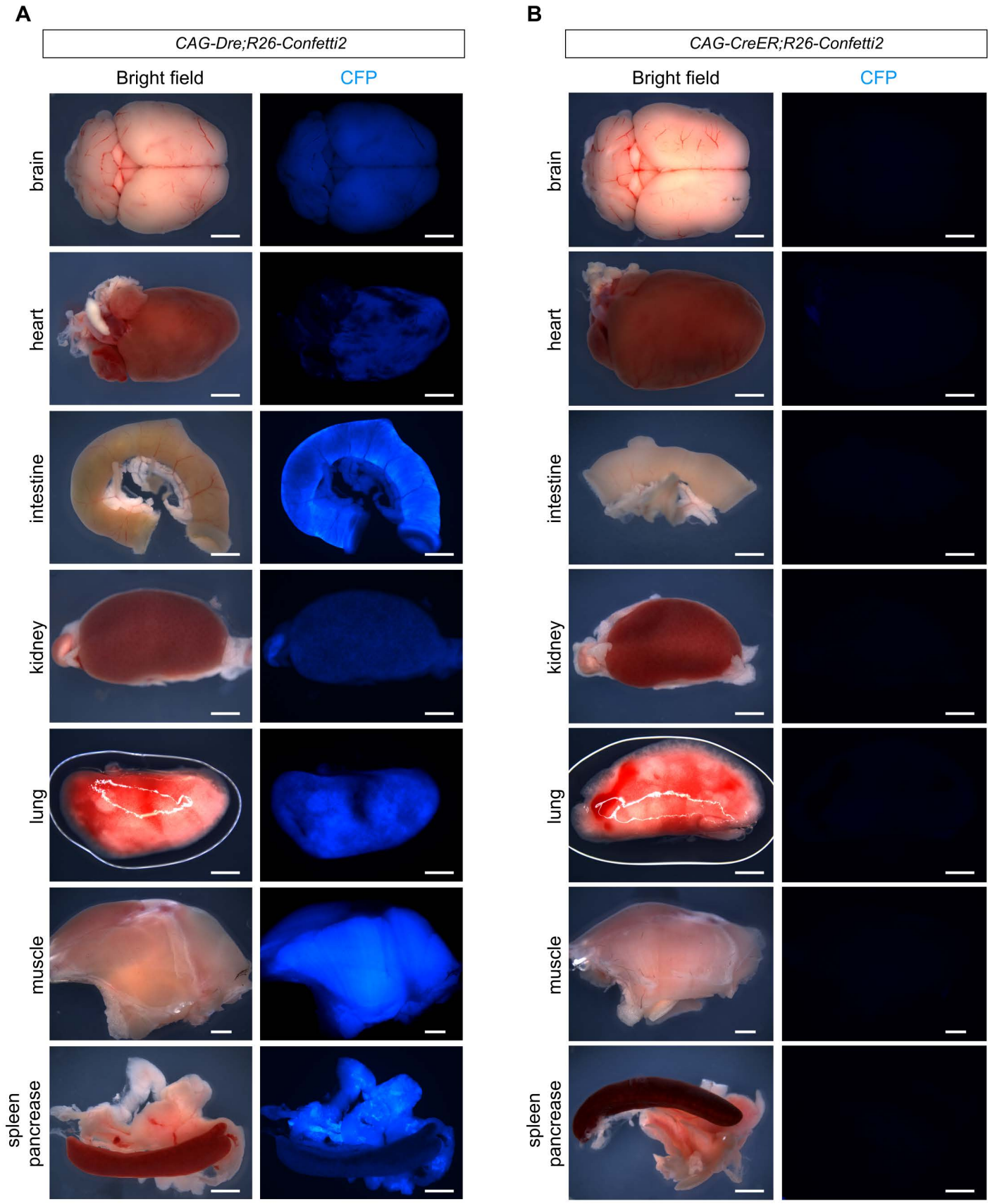

Figure S3: Examination of *R26-roxRB* by *CAG-Dre* or *CAG-CreER*, related to Figure 5
(A) The leaky of *CAG-Dre;R26-Confetti2* and *CAG-CreER;R26-Confetti2* mice. As the data indicates, *CAG-Dre;R26-Confetti2* mice were CYP^{+}, but GFP^{-},RFP^{-} and YFP^{-}.
(B) While *CAG-CreER;R26-Confetti2* mice were no signal. Tamoxifen was induced two days before tissue collection. Scale bars, 2 mm. Each image is representative of 5 individual samples.

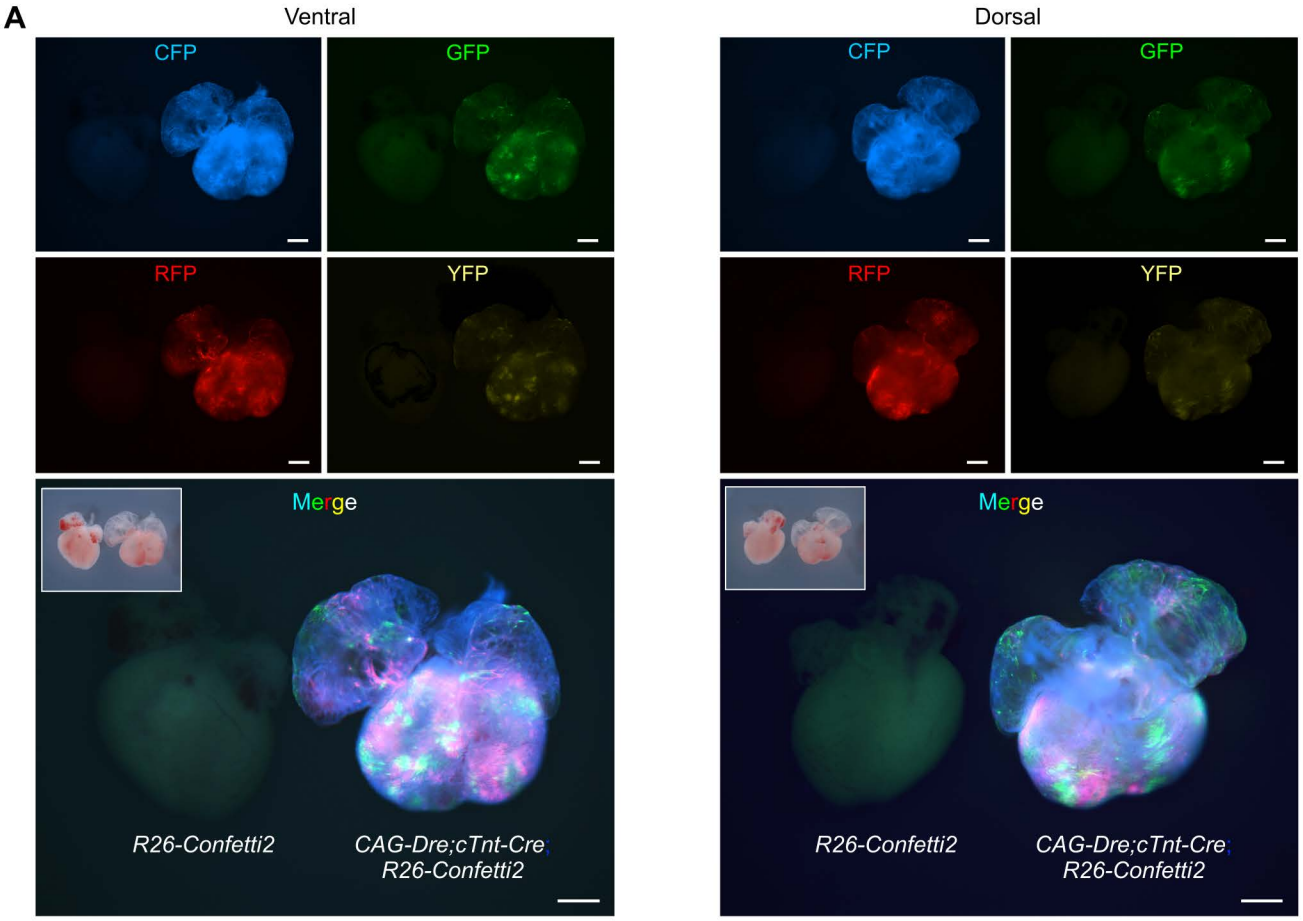

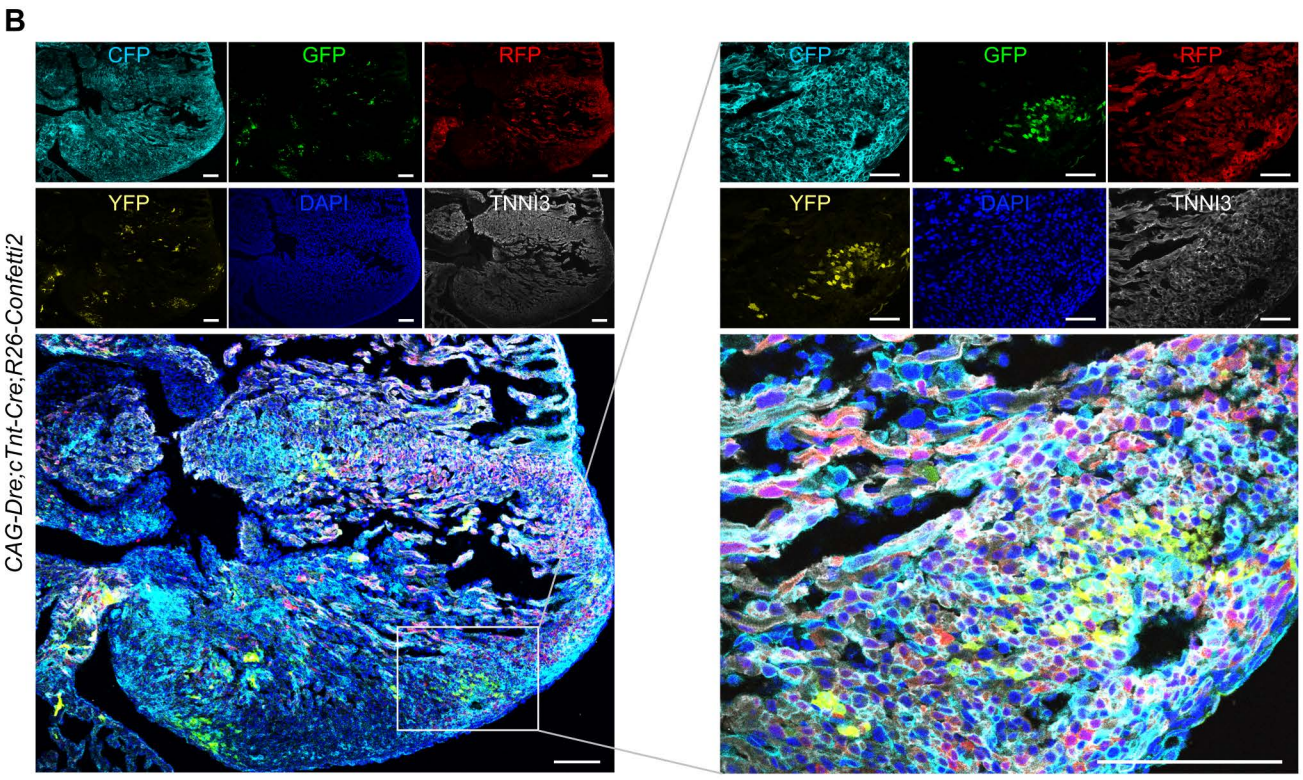

Figure S4: Characterization of *R26-Confetti2* in mouse heart, related to Figure 5
(A) Whole-mount fluorescence images of hearts collected from E18.5 *CAG-Dre;cTnt-Cre;R26-Confetti2* or littermate control *R26-Confetti2* embryos. Inserts are bright-field images.
(B) Fluorescent image of section stained with TNNI3 shows expression of GFP, RFP and YFP in TNNI3^{+} cardiomyocytes. Sclae bars, 500 μm in **(A)**; 100 μm in **(B)**.

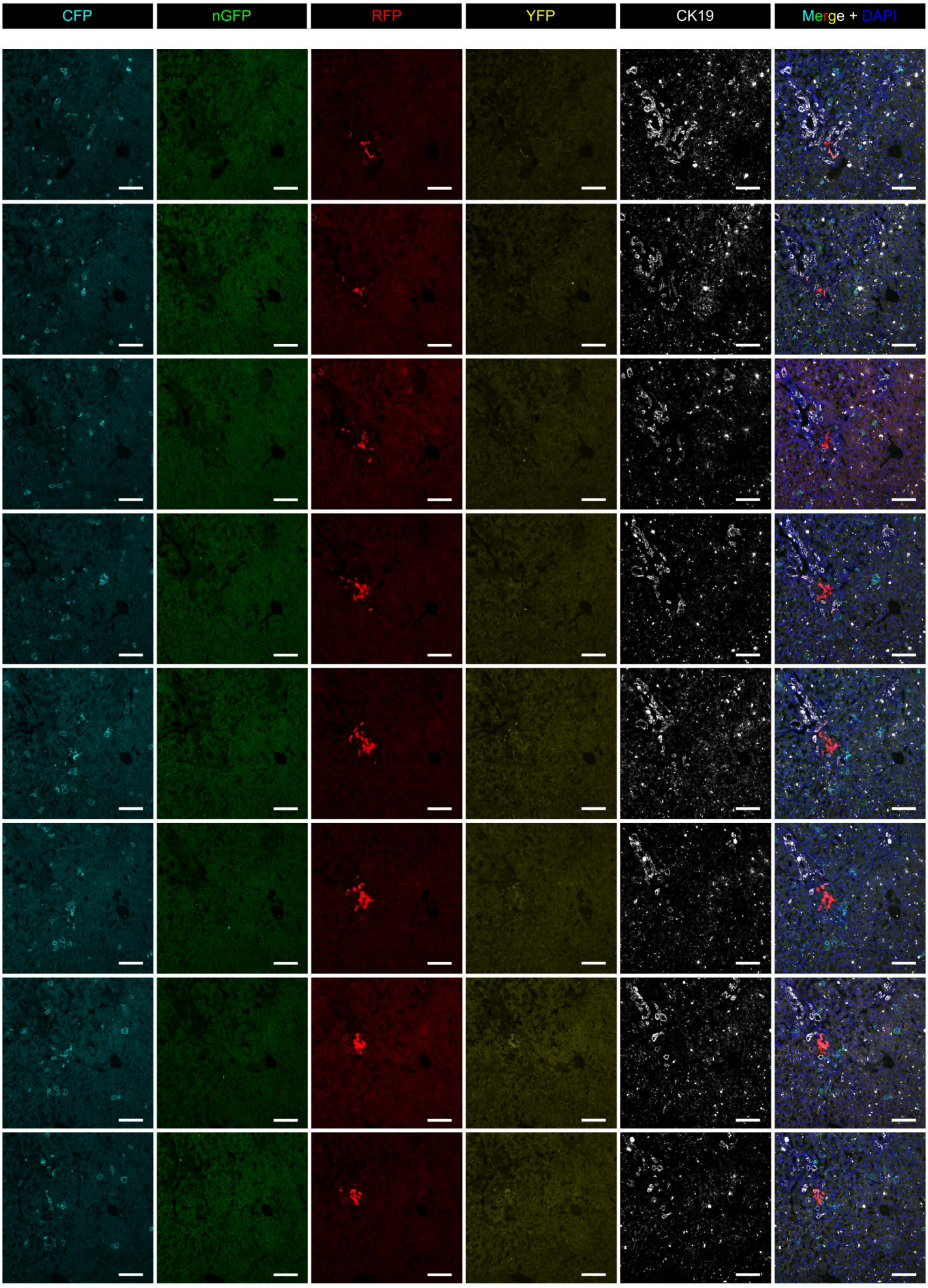

Figure S5: Zoom out fluorescent sections of Figure 6 stained with BEC marker CK19. Slide 1-8 are serial sections. Scale bars, 100 µm, related to Figure 6

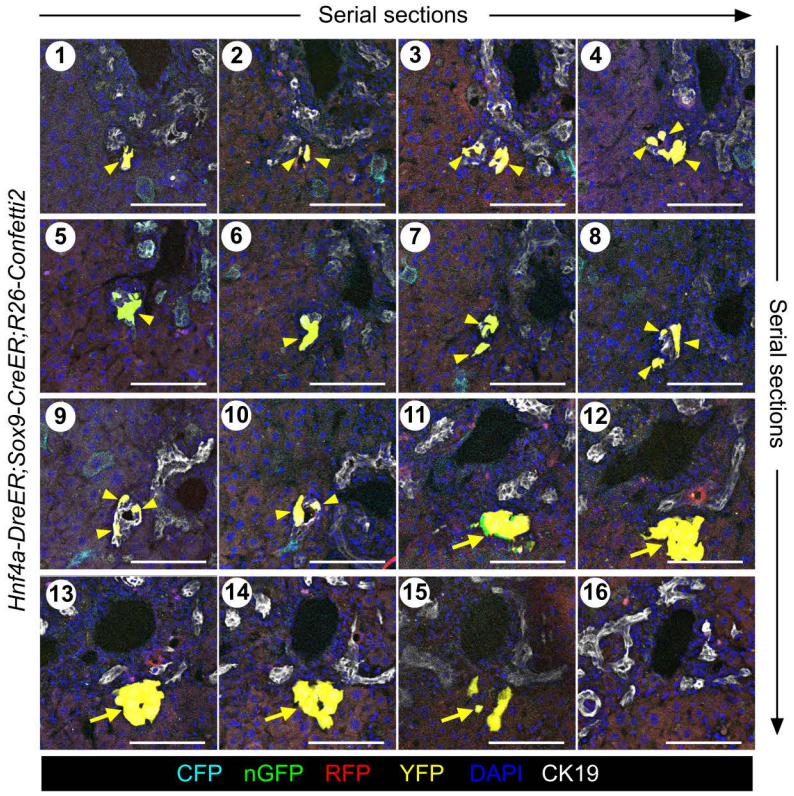

Figure S6: Additional bi-potent clone in serial sections after liver injury , related to Figure 6
Another fluorescent sections of a bi-potent clone that contains both BECs (arrowheads) and hepatocytes (arrows) stained with BEC marker CK19. Slide 1-16 are serial sections. Scale bars, 100 μm.

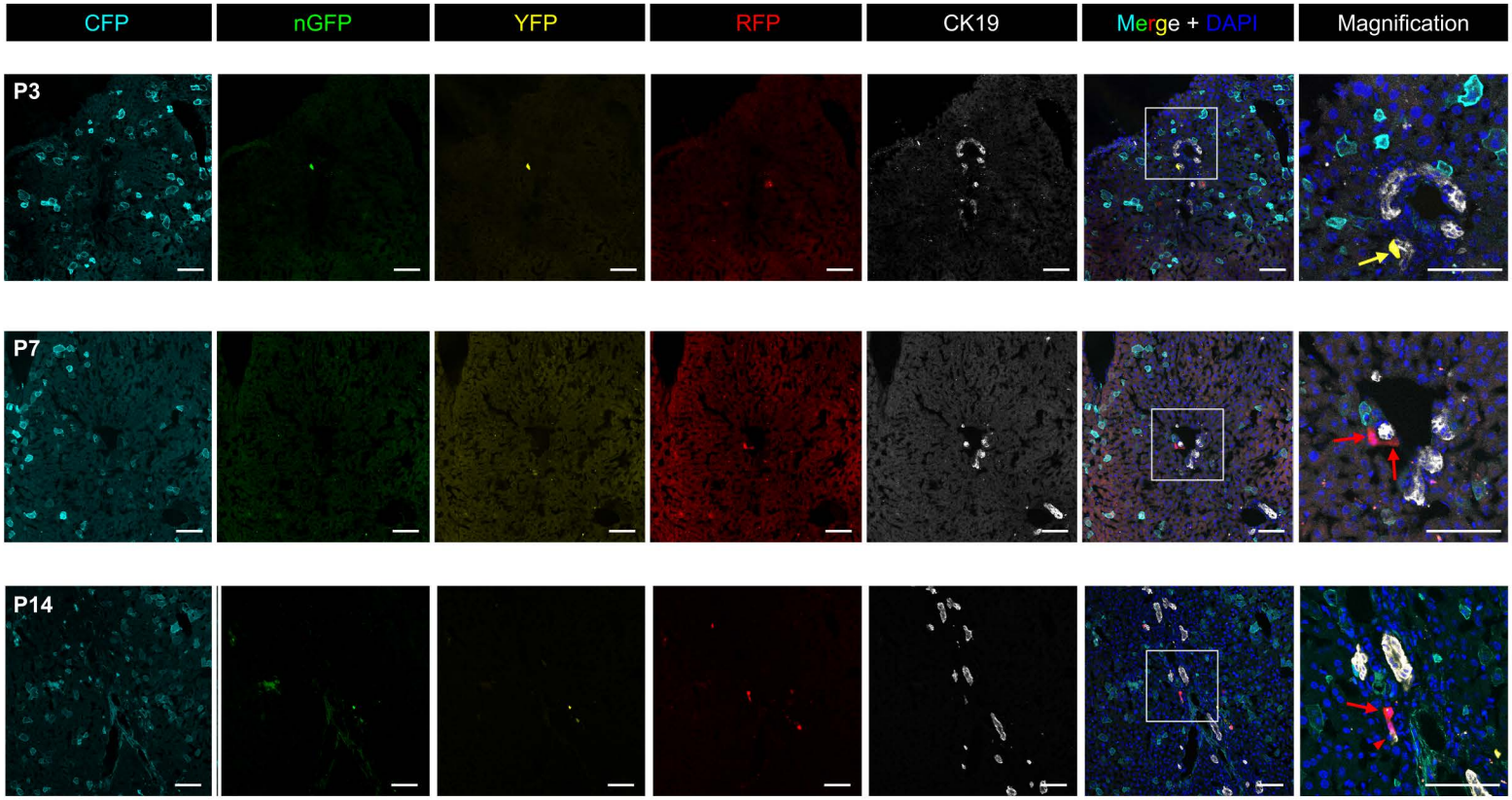

Figure S7: Clonal analysis of SOX9⁺ hepatocyte at early stages after BDL, related to Figure 6
Fluorescent sections stained with BEC marker CK19 shows only hepatocytes (arrows) at post-BDL day 3 (P3) or P7. Double hepatocyte could be detected at P7 (arrowheads). Only at P14 could we detect both hepatocyte (arrow) and BEC (arrowhead) in clone. Scale bars, 100 μm.

SUPPLEMENTAL EXPERIMENTAL PROCEDURES

Mice

All mouse studies were carried out strictly according to the guidelines of the Institutional Animal Care and Use Committee (IACUC) at the Institute of Biochemistry and Cell Biology and the Institute for Nutritional Sciences, Shanghai Institutes for Biological Sciences, Chinese Academy of Sciences. *Hnf4a-DreER* was generated by CRISPR/Cas9 through homologous recombination. A complementary cDNA encoding IRES-DreER^{T2} was inserted in-frame with the translation codon of the *Hnf4a* gene. The chimeric mice positive for targeted ES cells were germ line transferred to F1 generation and bred on a C57BL/6 x ICR background. The *Sox9-CreER^{T2}* line was generated by the National Institute for Biological Sciences, Beijing, China. *R26-Ai66* (*Rosa26-rox-Stop-rox-loxP-Stop-loxP-tdTomato*) as reported previously (Madisen et al., 2015; Zhang et al., 2016). The *Rosa26-Rox-Stop-Rox-tdTomato* (*R26-RSR-RFP*) mouse line was generated by crossing *ACTB-Cre* with *R26-Ai66* to excise the second loxP-flanked Stop cassette, and *ACTB-Cre* was not passaged to the subsequent mouse breeding. *R26-RSR-RFP* was responsive to Dre but not Cre recombinase. The *Rosa26-rox-Stop-rox-Confetti* (*R26-Confetti2)* was generated by targeting CAG-rox-stop-rox-Confetti cassette into the Rosa26 gene locus by homologous recombination (Figure 5A). All experimental mice were maintained on a C57BL6/ICR mixed background. Tamoxifen (Sigma, T5648) was dissolved in corn oil (20 mg/ml) and administered by gavage at the indicated time points. We treated *R26-RFP* and *R26-Confetti2* mice with 0.4 mg tamoxifen/g of mouse body weight (mg/g) and 0.15 mg/g tamoxifen respectively.

Genomic PCR

Genomic DNA was prepared from mice tail. Tails were lysed by incubation with Proteinase K overnight at 55 °C, followed by centrifugation at maximum speed for 8 min, to obtain supernatant with genomic DNA. DNA was precipitated by adding isopropanol and washed in 70% ethanol, and was finally dissolved in distilled H2O. All mice were genotyped with specific primers that distinguish knock-in allele from wild-type allele. For the *R26-RSR-RFP* line, primers 5'-ACGGGTGTTGGGTCGTTTGTTC-3' and 5'-TTCTTGTAATCGGGGATGTCGGCG-3 were used to detect the tdTomato positive allele, and 5'-AAGGGAGCTGCAGTGGAGTA-3'and 5'-CCGAAAATCT- GTGGGAAGTC-3' were used to detect the wild-type allele. For the *Hnf4a-DreER* line, primes 5'- GCTCTGGTGGTCTGCTCTGA-3' and 5'-CCCTTGTTGAATACGCTTGA-3' were used to detect the DreERT2 positive allele, and 5'-GCTCTGGTGGTCTGCTCTGA-3' and 5'- CTGGCCTTGAATGTCTGGAA-3' were used to detect the wild-type allele. For the *Sox9-CreERT2* line, primers 5'-GCAAAAGTATTACATCACGGGGG-3' and 5'-ACAAAGTCCAAACAGGCAGGG-3' were used to detect the CreER positive allele, and 5'-GTAAAGGAAGGTAACGATTGCTGG-3' and 5'- ACAAAGTCCAAACAGGCAGGG-3' were used to detect the wild-type allele. For the *R26-LSL-RFP* line, primers 5'-GGCATTAAAGCAGCGTATCC-3' and 5'-CTGTTCCTGTACGGCATGG-3' were used to detect the tdTomato positive allele, and 5'-AAGGGAGCTGCAGTGGAGTA-3' and 5'-CCGAAAATCTGTGGGAAGTC-3' were used to detect the wild type allele. For the *R26-Confetti2* line, primes 5'- TGCTGTGCTGCATCAGAAGAAC-3' and 5'-TGCTTGTCGGCGGTGATATAG-3' were used to detect the CFP positive allele, and 5'-TTGGAGGCAGGAAGCACTTG-3' and 5'- CCGACAAAACCGAAAATCTGTG-3' were used to detect the wild-type allele.

Injury Model

For the CCl4 induced chronic injury model, CCl4 was dissolved at 1:3 in corn oil and injected intraperitoneally at a dose of 4 μl/g body weight every 3 days for 10 times. Partial hepatectomy (PHx) was generated by removing two thirds of the liver to induce the injury. For details, 8 week old mice were anaesthetized with 2% isoflurane and oxygen flow in a plexiglass chamber. The abdominal fur was removed and the skin was disinfected. The mice were transferred onto a 37 °C heat pad and maintained anesthesia by inhalation of isoflurane with oxygen. A midline abdominal skin and muscle incision was made to expose the liver. The left lobe and the median lobe were tied and cut. The peritoneum was closed with a 5–0 suture and skin was closed afterwards. After closing the abdomen, the skin surrounding the suture was disinfected with betadine and the animal was placed on a warming pad for recovery. BDL injury model was carried out according to established protocols described previously (Pu et al., 2016). Anesthesia procedure was the same as PH. A midline abdominal incision was made to expose the liver. The common bile duct was ligated twice with 4–0 silk sutures. Sham-operated animals were used as controls. For DDC induced chronic injury model, mice received mouse diet (Harlan Teklad, 5015) containing 0.1% DDC (Sigma-Aldrich).

Whole-mount Fluorescence Microscopy

Collected mouse liver was washed in PBS and placed on agar for the whole mount bright field and fluorescence imaging using the Zeiss (AxioZoom V16). To determine magnification of specific regions, we used the automated Z-stack images acquired by the Zeiss stereo-scope (AxioZoom V16).

Immunostaining

Immunostaining was performed according to the standard protocols described previously (Tian et al., 2013). For details, tissues were dissected in PBS and fixed in 4% paraformaldehyde (PFA Sigma) at 4 °C for 45-60 min. Afterwards, tissues were washed in PBS 5 min for three times, dehydrated in 30% sucrose overnight at 4 °C. Following an hour of immersion in optimum cutting temperature (O.C.T., Sakura) at 4 °C, the liver was embedded in blocks and frozen at −80 °C. Sections of 8-10 μm thickness were collected on slides and air dried afterwards at room temperature at least 2 hours. For immunostaining, dried sections were washed in PBS 5 min for three times and then blocked with 5% normal donkey serum (Jackson Immunoresearch) and 0.1% Triton X-100 in PBS for 30 min at room temperature. Sections were incubated with the primary antibodies overnight at 4 °C. The following antibodies were used: RFP (Rockland, 600-401-379, 1:200), HNF4a (Santa Cruz, sc-6556, 1:100), cytokeratin 19 (CK19, Developmental Studies Hybridoma Bank, TROMA-III, 1:100), VE-cadherin (R&D, AF1002, 1:100), Desmin (R & D, AF3844, 1:100), PDGFR (R&D, AF1062, 1:100), E-cadherin (Cell Signaling, 3195, 1:100), EpCAM (Abcam, ab92383, 1:100), SMA (Sigma, F3777, 1:100), Ki67 (Thermo scientific, RM-9106 - S0, 1:100). Signals were developed with Alexa fluorescence antibodies (Invitrogen), and nuclei were counterstained with 4'6-diamidino-2-phenylindole (DAPI, Vector lab). For clonal analysis, CK19 was stained on the liver sections in far red channel. Totally 246 clones were analyzed: 820 cholangiocytes in cholangiocyte clones; 412 hepatocytes in hepatocyte clones; 156 cholangiocytes and 66 hepatocytes in mixed clones. And there was bleed-through of fluorescence for YFP and GFP, as this was due to YFP signal could also be detected in the GFP channel. In addition, our GFP is nGFP (nuclear), so pure GFP signal should be in the nucleus; while bleed-through signal in the GFP channel from YFP should not be nuclear signal. Immunostaining images were acquired by Olympus fluorescence microscope (BX53), Zeiss stereomicroscope (AXIO Zoom, V16), Zeiss confocal laser scanning microscope (LSM510) and Olympus confocal microscope (FV1200).

Sirius Red Staining

Sirius red staining was aimed to assess fibrotic tissue after chronic injury models. For details, cryosections were washed in PBS for 15 min and then fixed in 4% paraformaldehyde (PFA Sigma) for 15 min. Slides were then washed with PBS for 15 min and fixed overnight in Bouins solution (5% acetic acid, 9% formaldehyde and 0.9% picric acid) at room temperature or 1 hour in 55°. Subsequently, the slides were washed in running tap water until the yellow color developed. Slides were stained with 0.1% Fast Green (Fisher) for 2.5-3 min and incubated in 1% acetic acid for 1 min followed by incubation with 0.1% Sirius red (Sigma) for 1-1.5 min; followed by rinsing with tap water before incubation into the staining solution. Finally, slides were dehydrated in 100% ethanol twice, cleared in xylene and covered with resinous medium. Images were obtained on an Olympus microscope (BX53).

Statistics

All data were collected from at least five independent experiments as indicated. Data for two groups were analyzed by a two-sided unpaired Student's t-test, whereas comparison between more than two groups was performed using an analysis of variance followed by Tukey's multiple comparison tests. Significance was accepted when $P < 0.05$. All data were presented as mean value ± SEM.

Data Availability

Data supporting the findings of this study are available within the article and its Supplementary Information files, and from the corresponding author upon reasonable request.

SUPPLEMENTAL REFERENCES

Miyajima, A., Tanaka, M., and Itoh, T. (2014). Stem/progenitor cells in liver development, homeostasis, regeneration, and reprogramming. Cell Stem Cell 14, 561-574.

Michalopoulos, G.K., Barua, L., and Bowen, W.C. (2005). Transdifferentiation of rat hepatocytes into biliary cells after bile duct ligation and toxic biliary injury. Hepatology 41, 535-544.

Pu, W., Zhang, H., Huang, X., Tian, X., He, L., Wang, Y., Zhang, L., Liu, Q., Li, Y., Li, Y., Zhao, H., Liu, K., Lu, J., Zhou, Y., Huang, P., Nie, Y., Yan, Y., Hui, L., Lui, K. O., and Zhou, B. (2016). Mfsd2a+ hepatocytes repopulate the liver during injury and regeneration. Nat Commun 7, 13369.

Tarlow, B. D., Pelz, C., Naugler, W. E., Wakefield, L., Wilson, E. M., Finegold, M. J., and Grompe, M. (2014b). Bipotential adult liver progenitors are derived from chronically injured mature hepatocytes. Cell Stem Cell 15, 605-618.